

UNIVERSIDAD SAN FRANCISCO DE QUITO

USFQ

Colegio de Ciencias e Ingenierías

**Plasmonic response of a metal nanoparticle in a gain
medium**

Daniel Alejandro Bustamante López

Física

Trabajo de titulación presentado como requisito para la obtención del título de

Licenciado en Física

Quito, 22 de diciembre de 2020

UNIVERSIDAD SAN FRANCISCO DE QUITO USFQ

Colegio de Ciencias e Ingenierías

**HOJA DE CALIFICACIÓN DE TRABAJO DE
TITULACIÓN**

Plasmonic response of a metal nanoparticle in a gain medium

Daniel Alejandro Bustamante López

Nombre del profesor, Título académico: Alessandro Veltri, Ph. D.

Quito, 22 de diciembre de 2020

© DERECHOS DE AUTOR

Por medio del presente documento certifico que he leído todas las Políticas y Manuales de la Universidad San Francisco de Quito USFQ, incluyendo la Política de Propiedad Intelectual USFQ, y estoy de acuerdo con su contenido, por lo que los derechos de propiedad intelectual del presente trabajo quedan sujetos a lo dispuesto en esas Políticas.

Asimismo, autorizo a la USFQ para que realice la digitalización y publicación de este trabajo en el repositorio virtual, de conformidad a lo dispuesto en la Ley Orgánica de Educación Superior del Ecuador.

| | |
|----------------------|-----------------------------------|
| Nombres y apellidos: | Daniel Alejandro Bustamante López |
| Código: | 00138295 |
| Cédula de Identidad: | 1720440120 |
| Lugar y fecha: | Quito, 22 de diciembre de 2020 |

ACLARACIÓN PARA PUBLICACIÓN

Nota: El presente trabajo, en su totalidad o cualquiera de sus partes, no debe ser considerado como una publicación, incluso a pesar de estar disponible sin restricciones a través de un repositorio institucional. Esta declaración se alinea con las prácticas y recomendaciones presentadas por el Committee on Publication Ethics COPE descritas por Barbour et al. (2017) Discussion document on best practice for issues around theses publishing, disponible en <http://bit.ly/COPETheses>.

UNPUBLISHED DOCUMENT

Note: The following capstone project is available through Universidad San Francisco de Quito USFQ institutional repository. Nonetheless, this project – in whole or in part – should not be considered a publication. This statement follows the recommendations presented by the Committee on Publication Ethics COPE described by Barbour et al. (2017) Discussion document on best practice for issues around theses publishing available on <http://bit.ly/COPETheses>.

RESUMEN

En este trabajo, se estudia la respuesta plasmónica de una nanopartícula de plata inmersa en un medio dieléctrico con elementos de ganancia. Se usa el formalismo cuántico de Bloch para describir la dinámica del medio activo y un tratamiento clásico es empleado para la interacción del metal con los campos. El modelo, dependiente de la geometría del sistema (en este caso, una nanoesfera), permite describir la evolución temporal de los campos electromagnéticos y el acoplamiento de los modos multipolares de la nanopartícula.

Palabras clave: Plasmónica, Nanopartícula metálica, Medio de ganancia.

ABSTRACT

In this work, the plasmonic response of a silver nanoparticle immersed in a dielectric medium with gain elements is studied. Bloch's quantum formalism is used to describe the dynamics of the active medium and a classical treatment is used for the interaction of metal with fields. The model, dependent on the geometry of the system (in this case, a nanosphere), allows describing the temporal evolution of electromagnetic fields and the coupling of the multipolar modes of the nanoparticle.

Keywords: Plasmonic, Metallic nanoparticle, Gain medium.

AGRADECIMIENTOS

A mi familia. Gracias por todo su esfuerzo y apoyo incondicional.

A mis profesores, quienes me brindaron su conocimiento y experiencia para formarme como científico. Un agradecimiento especial a mi supervisor Alessandro Veltri por su guía a lo largo de mi carrera universitaria y por haberme inspirado a trabajar en este proyecto de tesis.

Contents

| | | |
|-----------|---|-----------|
| 1 | Introduction | 12 |
| 2 | Vector Spherical Harmonics | 13 |
| 3 | Electric and Magnetic Fields | 15 |
| 4 | Free Electron Model | 19 |
| 5 | Optical Bloch Equations | 21 |
| 6 | Boundary Conditions | 25 |
| 7 | Numerical Resolution of Equations | 27 |
| 8 | Linear Amplification Regime | 30 |
| 9 | Nonlinear Regime | 41 |
| 10 | Conclusions | 54 |
| 11 | Future Work | 54 |
| 12 | Appendices | 57 |
| 12.1 | Code to obtain the temporal evolution of the fields | 57 |
| 12.2 | Example of input file | 76 |

List of Figures

| | | |
|---|--|----|
| 1 | Scattering of light by a sphere. A spherical nanoparticle made of metal is immersed in a dielectric medium with active dipole elements (red dots). The radius of the nanoparticle is a . | 16 |
| 2 | Temporal evolution of N for $G = -0.01$. Eventually, $N \approx \tilde{N}$ is obtained when the value of G is relatively small, without dependence on the θ and ϕ coordinates. We assume a large fixed power for the pump: $\tilde{N} = 1$. | 31 |
| 3 | Plasmonic response of a 10 [nm] silver nanoparticle as gain is increased in the surrounding medium. Parameters: $\varepsilon_b = 1.8496\varepsilon_0$ (ethanol solvent), $\hbar\omega_{21} = 3.2$ [eV], $\Delta = 0.2$ [eV]. | 32 |
| 4 | Time evolution of $ \mathbf{E} ^2 / \overline{ \mathbf{E}_0 ^2}$ at different points on the surface of the sphere when $G = -0.01$ and $\omega = \omega_{21}$. $\mathbf{E} = \mathbf{E}_{(2)}$ is the external electric field. $\overline{ \mathbf{E}_0 ^2}$ is the average of $ \mathbf{E}_{(2)} ^2$ on the surface of the sphere when $G = 0$. | 33 |
| 5 | Time evolution of $ \mathbf{E}_{\text{quadrupole}} ^2 / \overline{ \mathbf{E}_0 ^2}$ at different points on the surface of the sphere when $G = -0.01$ and $\omega = \omega_{21}$. In $ \mathbf{E}_{\text{quadrupole}} ^2$ only the terms with $J = 2$ are taken into account during the calculation of the external electric field, which corresponds to the quadrupole term of the field. | 33 |
| 6 | Time evolution of $ \boldsymbol{\Pi}_{(2)} ^2 / \overline{ \varepsilon_0 \mathbf{E}_0 ^2}$ when $G = -0.01$ and $\omega = \omega_{21}$. | 34 |
| 7 | Time evolution of $\Im(\mathbf{E} \cdot \boldsymbol{\Pi}_{(2)}^*) / (\varepsilon_0 \overline{ \mathbf{E}_0 ^2})$ when $G = -0.01$ and $\omega = \omega_{21}$. $\mathbf{E} = \mathbf{E}_{(2)}$ is the external electric field. | 34 |

| | | |
|----|---|----|
| 8 | Plasmonic response for values of G for which the system goes into a nonlinear amplification regime. An easy rule of thumb to predict the extent of the linear amplification regime is to look for a sign change in the imaginary part of the polarizability (compare with Fig. 3) [8]. | 35 |
| 9 | When the gain value exceeds a threshold and the system goes into a nonlinear regime, the dipolar approximation of the plasmonic response is no longer valid. | 36 |
| 10 | Evolution of the permittivities in the metal and the gain medium for $G = -0.01$ and $\omega = \omega_{21}$. The permitivities converge to the values given by equations 4.9 and 5.15. | 37 |
| 11 | A close inspection of the temporal evolution of N , showing that it converges approximately to \tilde{N} . This result is shown at two points on the surface of the nanosphere. | 38 |
| 12 | A close inspection of the temporal evolution of $ \mathbf{E} ^2$, showing that it converges. This result is shown at two points on the surface of the nanosphere. It is observed that the external electric field is more intense when $\theta = 90^\circ$ and $\phi = 0^\circ$, which corresponds to the pole of the nanosphere that is on the x -axis, the axis that has the same direction as the incident electric field. | 39 |
| 13 | A close inspection of the temporal evolution of $ \boldsymbol{\Pi}_{(2)} ^2$ shows that it converges. | 39 |
| 14 | A close inspection of the temporal evolution of $\Im(\mathbf{E} \cdot \boldsymbol{\Pi}_{(2)}^*)$ shows that it converges. The relatively small magnitude of this quantity explains why N converges to values close to \tilde{N} , as indicated by equation 5.7. | 40 |
| 15 | When G is small, the plasmonic response is basically dipolar and the electric field is strongest at the poles that are on the axis that has the same direction as the incident electric field. | 40 |

| | | |
|----|---|----|
| 16 | Temporal evolution of N for $G = -1$ and $\omega = \omega_{21}$. In the nonlinear regime, N no longer converges to a value approximately equal to \tilde{N} due to the competitive effect imposed by the term on the right hand side of equation 5.7 (which can be understood as a negative source term, no longer negligible as in the linear case, that causes the population inversion to be depleted). | 41 |
| 17 | Evolution of the permittivities in the metal and the gain medium for $G = -1$ and $\omega = \omega_{21}$ | 42 |
| 18 | Time evolution of $ \mathbf{E} ^2 / \overline{\mathbf{E}_0} ^2$ when $G = -1$ and $\omega = \omega_{21}$ | 42 |
| 19 | Time evolution of $ \mathbf{E}_{\text{quadrupole}} ^2 / \overline{\mathbf{E}_0} ^2$ when $G = -1$ and $\omega = \omega_{21}$. In $ \mathbf{E}_{\text{quadrupole}} ^2$ only the terms with $J = 2$ are taken into account, which corresponds to the quadrupole term of the external field. | 43 |
| 20 | Time evolution of $ \Pi_{(2)} ^2 / \overline{\varepsilon_0 \mathbf{E}_0} ^2$ when $G = -1$ and $\omega = \omega_{21}$. $\mathbf{E} = \mathbf{E}_{(2)}$ and $\Pi_{(2)}$ are the electric field and the non-linear polarization term in the gain medium. | 43 |
| 21 | Time evolution of $\Im(\mathbf{E} \cdot \Pi_{(2)}^*) / (\varepsilon_0 \overline{\mathbf{E}_0} ^2)$ when $G = -1$ and $\omega = \omega_{21}$. $\mathbf{E} = \mathbf{E}_{(2)}$ and $\Pi_{(2)}$ are the electric field and the non-linear polarization term in the gain medium. | 44 |
| 22 | A close inspection of the temporal evolution of $ \mathbf{E} ^2$ and N shows that these quantities eventually oscillate with constant period. Also, when $ \mathbf{E} ^2$ has a maximum, N has a minimum. | 45 |

| | | |
|----|---|----|
| 23 | Difference between $ \mathbf{E}(\theta = 90^\circ, \phi = 0^\circ) ^2$ and $ \mathbf{E}(90^\circ, 90^\circ) ^2$. In the linear case, the energy was mostly concentrated at the poles of the sphere along the x -axis (the direction of the incident electric field). However, in this plot we note that, in certain periods of time, the field loses intensity along the x -axis to concentrate at other points on the surface of the nanosphere: at points on the plot where the difference is negative (blue), the electric field is more intense at the poles along the y -axis with respect to the poles along the x -axis. This is a sign of the emergence of other multipolar modes (see Fig. 28 to notice the momentary disappearance of the dipole character of the plasmonic response). | 46 |
| 24 | Difference between $ \mathbf{E}(90^\circ, 0^\circ) ^2$ and $ \mathbf{E}(0^\circ, 0^\circ) ^2$. At points on the plot where the difference is negative (blue), the electric field is more intense at the poles along the z -axis with respect to the poles along the x -axis. | 47 |
| 25 | A close inspection of the temporal evolution of $ \Pi_{(2)} ^2$ shows that it oscillates. . . . | 48 |
| 26 | A close inspection of the temporal evolution of $\Im(\mathbf{E} \cdot \Pi_{(2)}^*)$ shows that it oscillates. This term in Bloch's equation is initially insignificant and N is quickly driven to \tilde{N} because population inversion is continually restored; the pump can repopulate the upper level continuously. However, this term gets larger eventually, which means that the population inversion of the gain elements is depleted due to the energy absorbed by the plasmonic field. | 49 |
| 27 | A closer inspection of the temporal evolution of the permitivities in the gain medium and in the metallic sphere. | 50 |

| | | |
|----|---|----|
| 28 | The plasmonic response is initially dipole, as is the case for small values of G . However, as the saturation process takes place, the dipolar mode is dissipated in parassite modes. | 51 |
| 29 | Continuation of Fig. 28. | 52 |
| 30 | Continuation of Fig. 29. | 53 |

1 Introduction

Metallic nanostructures attract a lot of interest in different fields of nanotechnology because they can sustain localized surface plasmon resonances, which originate from the collective oscillation of their electrons in response to an electromagnetic excitation [1]. This property makes these systems have the ability to concentrate light and produce local fields of high intensity, allowing to manipulate the light and enhance linear and non-linear phenomena [2]. For this reason, multiple efforts are being made to control, amplify, and tune the localized surface plasmon resonances for different purposes [3].

In this work, we consider a homogeneous metallic nanosphere (as illustrated in Fig. 1), which is embedded in a gain medium, formed by a dielectric host with dispersed active elements (e.g., a solution of quantum dots). At optical frequencies, the use of gain is intended to overcome energy losses in the system by metal absorption [4]. This is a simple geometry that we will use to quantitatively describe the phenomenon of surface plasmon amplification. The interest of coupling metallic nanostructures with the active media is inspired by the realization of the SPASER (acronym for Surface Plasmon Amplification by Stimulated Emission of Radiation), which would be the plasmonic equivalent of a laser and would allow the confinement of light at a subwavelength scale, eliminating the problem of the diffraction limit of light [5]. The SPASER at the same time is attractive for its potential use in applications such as nanoscale lithography, microscopy, optoelectronics, subwavelength focusing and solution for losses in next-generation active metamaterials [6][7].

To advance in the fundamental understanding of SPASERs, it is very important to develop precise theoretical descriptions of the plasmonic phenomena associated with the system that we will study. In recent years, several works have appeared on the optical properties of gain-assisted nanoparticles with various geometries. However, these works were carried out in stationary regimes for both the nanoparticle and the surrounding gain medium or are based in simplified time-dependent models, which start from assumptions such as that the plasmonic response of the nanosphere is dipolar [8]. Such simplifications are acceptable to some extent, but plasmon amplification is not always stationary or dipolar and complex time-dependent effects can arise from these systems. Consequently, this work seeks a broader description of SPASER that characterizes non-stationary regimes and the mechanisms of emergence of multipolar modes.

2 Vector Spherical Harmonics

The vector spherical harmonics are vector fields that can be considered as an extension of the scalar spherical harmonics. Given a scalar spherical harmonic $Y_{J,M}(\theta, \phi)$, we define three vector spherical harmonics [9]:

$$\mathbf{Y}_{J,M}^{(-1)}(\theta, \phi) = Y_{J,M}(\theta, \phi)\mathbf{n}, \quad (2.1)$$

$$\mathbf{Y}_{J,M}^{(0)}(\theta, \phi) = \frac{-i}{\sqrt{J(J+1)}} (\mathbf{n} \times \nabla_\Omega) Y_{J,M}(\theta, \phi), \quad (2.2)$$

$$\mathbf{Y}_{J,M}^{(1)}(\theta, \phi) = \frac{1}{\sqrt{J(J+1)}} \nabla_\Omega Y_{J,M}(\theta, \phi), \quad (2.3)$$

where $\mathbf{n} = \mathbf{r}/r$ and ∇_Ω denotes the angular part of the ∇ operator.

The components of the vector spherical harmonics are

$$\left[\mathbf{Y}_{J,M}^{(-1)}(\theta, \phi) \right]_r = Y_{J,M}(\theta, \phi), \quad (2.4)$$

$$\left[\mathbf{Y}_{J,M}^{(-1)}(\theta, \phi) \right]_\theta = 0, \quad (2.5)$$

$$\left[\mathbf{Y}_{J,M}^{(-1)}(\theta, \phi) \right]_\phi = 0, \quad (2.6)$$

$$\left[\mathbf{Y}_{J,M}^{(0)}(\theta, \phi) \right]_r = 0, \quad (2.7)$$

$$\left[\mathbf{Y}_{J,M}^{(0)}(\theta, \phi) \right]_\theta = \frac{-M}{\sqrt{J(J+1)}} \frac{1}{\sin \theta} Y_{J,M}(\theta, \phi), \quad (2.8)$$

$$\begin{aligned} \left[\mathbf{Y}_{J,M}^{(0)}(\theta, \phi) \right]_\phi &= -\frac{i}{2} \sqrt{\frac{(J-M)(J+M+1)}{J(J+1)}} e^{-i\phi} Y_{J,M+1}(\theta, \phi) \\ &\quad + \frac{i}{2} \sqrt{\frac{(J+M)(J-M+1)}{J(J+1)}} e^{i\phi} Y_{J,M-1}(\theta, \phi), \end{aligned} \quad (2.9)$$

$$\left[\mathbf{Y}_{J,M}^{(1)}(\theta, \phi) \right]_r = 0, \quad (2.10)$$

$$\begin{aligned} \left[\mathbf{Y}_{J,M}^{(1)}(\theta, \phi) \right]_\theta &= \frac{1}{2} \sqrt{\frac{(J-M)(J+M+1)}{J(J+1)}} e^{-i\phi} Y_{J,M+1}(\theta, \phi) \\ &\quad - \frac{1}{2} \sqrt{\frac{(J+M)(J-M+1)}{J(J+1)}} e^{i\phi} Y_{J,M-1}(\theta, \phi), \end{aligned} \quad (2.11)$$

$$\left[\mathbf{Y}_{J,M}^{(1)}(\theta, \phi) \right]_\phi = \frac{iM}{\sqrt{J(J+1)}} \frac{1}{\sin \theta} Y_{J,M}(\theta, \phi). \quad (2.12)$$

Furthermore, the vector spherical harmonics satisfy the following equations and algebraic relations

$$\nabla \times [f(r)\mathbf{Y}_{J,M}^{(-1)}(\theta, \phi)] = -i\sqrt{J(J+1)}\frac{1}{r}f(r)\mathbf{Y}_{J,M}^{(0)}(\theta, \phi), \quad (2.13)$$

$$\nabla \times [f(r)\mathbf{Y}_{J,M}^{(0)}(\theta, \phi)] = i\left(\frac{d}{dr} + \frac{1}{r}\right)f(r)\mathbf{Y}_{J,M}^{(1)}(\theta, \phi) + i\sqrt{J(J+1)}\frac{1}{r}f(r)\mathbf{Y}_{J,M}^{(-1)}(\theta, \phi), \quad (2.14)$$

$$\nabla \times [f(r)\mathbf{Y}_{J,M}^{(1)}(\theta, \phi)] = i\left(\frac{d}{dr} + \frac{1}{r}\right)f(r)\mathbf{Y}_{J,M}^{(0)}(\theta, \phi), \quad (2.15)$$

$$\mathbf{n} \times \mathbf{Y}_{J,M}^{(-1)}(\theta, \phi) = 0, \quad (2.16)$$

$$\mathbf{n} \times \mathbf{Y}_{J,M}^{(0)}(\theta, \phi) = i\mathbf{Y}_{J,M}^{(1)}(\theta, \phi), \quad (2.17)$$

$$\mathbf{n} \times \mathbf{Y}_{J,M}^{(1)}(\theta, \phi) = i\mathbf{Y}_{J,M}^{(0)}(\theta, \phi). \quad (2.18)$$

The interest in vector spherical harmonics lies in their ability to separate the radial from the angular dependence when spherical coordinates are used, so that a vector field (such as an electromagnetic field) can be expressed as a multipolar expansion.

3 Electric and Magnetic Fields

Our model was developed in several steps. First, the problem of electromagnetic scattering by a sphere is solved using Mie theory. In this way, electromagnetic fields near the surface of the sphere are calculated.

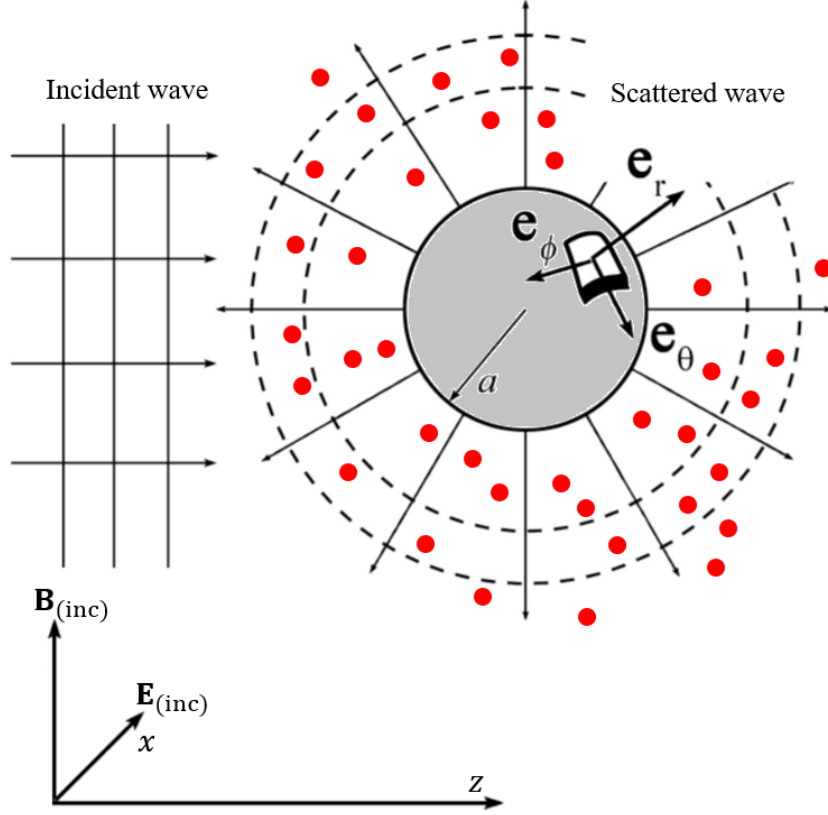


Figure 1: Scattering of light by a sphere. A spherical nanoparticle made of metal is immersed in a dielectric medium with active dipole elements (red dots). The radius of the nanoparticle is a .

We use the following expansion of the electromagnetic fields, $\mathbf{E}_{(i)}(\mathbf{r})$ and $\mathbf{B}_{(i)}(\mathbf{r})$, based on Bessel functions [10]:

$$\mathbf{E}_{(i)} = \frac{1}{2} \sum_{J,M} C_J \left[a_{J,M}^{(i)} f_J^{(i)} \mathbf{Y}_{J,M}^{(0)} + \alpha^{(i)} b_{J,M}^{(i)} \nabla \times \left(f_J^{(i)} \mathbf{Y}_{J,M}^{(0)} \right) \right], \quad (3.1)$$

$$c\mathbf{B}_{(i)} = \frac{1}{2} \sum_{J,M} C_J \left[b_{J,M}^{(i)} f_J^{(i)} \mathbf{Y}_{J,M}^{(0)} + \beta^{(i)} a_{J,M}^{(i)} \nabla \times \left(f_J^{(i)} \mathbf{Y}_{J,M}^{(0)} \right) \right], \quad (3.2)$$

where $C_J \equiv i^J \sqrt{4\pi(2J+1)}$, $\alpha^{(i)}(k^{(i)})$ and $\beta^{(i)}(k^{(i)})$ are constants that depend on the medium (the metallic sphere or the gain medium), $k^{(i)}$ is the wave vector norm, $f_J^{(i)}(k^{(i)}r)$ are Bessel functions, and $\mathbf{Y}_{J,M}^{(-1)}(\theta, \phi)$, $\mathbf{Y}_{J,M}^{(0)}(\theta, \phi)$, $\mathbf{Y}_{J,M}^{(1)}(\theta, \phi)$ are the vector spherical harmonics. i is an index to

denote that the field is incident ($i = \text{inc}$), scattered ($i = \text{sc}$), internal ($i = 1$) or external ($i = 2$).

For scattered and external fields, $f = h$ is the spherical Hankel function of the first kind. On the other hand, for incident and internal fields, $f = j$ is the spherical Bessel function of the first kind

The previous expression for the electric field can be rewritten for each of the fields as

$$\mathbf{E}_{(1)} = \frac{1}{2} \sum_{J,M} C_J \left[\left\{ \alpha^{(1)} b_{J,M}^{(1)} \frac{i}{r} \frac{d[rj_J^{(1)}]}{dr} \right\} \mathbf{Y}_{J,M}^{(1)} + \left\{ a_{J,M}^{(1)} j_J^{(1)} \right\} \mathbf{Y}_{J,M}^{(0)} + \left\{ \alpha^{(1)} b_{J,M}^{(1)} i \sqrt{J(J+1)} \frac{j_J^{(1)}}{r} \right\} \mathbf{Y}_{J,M}^{(-1)} \right], \quad (3.3)$$

$$\mathbf{E}_{(\text{inc})} = \frac{1}{2} \sum_{J,M} C_J \left[\left\{ \alpha^{(2)} b_{J,M}^{(\text{inc})} \frac{i}{r} \frac{d[rj_J^{(2)}]}{dr} \right\} \mathbf{Y}_{J,M}^{(1)} + \left\{ a_{J,M}^{(\text{inc})} j_J^{(2)} \right\} \mathbf{Y}_{J,M}^{(0)} + \left\{ \alpha^{(2)} b_{J,M}^{(\text{inc})} i \sqrt{J(J+1)} \frac{j_J^{(2)}}{r} \right\} \mathbf{Y}_{J,M}^{(-1)} \right], \quad (3.4)$$

$$\mathbf{E}_{(\text{sc})} = \frac{1}{2} \sum_{J,M} C_J \left[\left\{ \alpha^{(2)} b_{J,M}^{(\text{sc})} \frac{i}{r} \frac{d[rh_J^{(2)}]}{dr} \right\} \mathbf{Y}_{J,M}^{(1)} + \left\{ a_{J,M}^{(\text{sc})} h_J^{(2)} \right\} \mathbf{Y}_{J,M}^{(0)} + \left\{ \alpha^{(2)} b_{J,M}^{(\text{sc})} i \sqrt{J(J+1)} \frac{h_J^{(2)}}{r} \right\} \mathbf{Y}_{J,M}^{(-1)} \right]. \quad (3.5)$$

The case where the incident electric field $\mathbf{E}_{\text{(inc)}}$ is a plane wave that oscillates with frequency ω is studied. Thus, we have the following information on the constants and the nonzero coefficients:

$$a_{J,1}^{\text{(inc)}} = a_{J,-1}^{\text{(inc)}} = 1, b_{J,1}^{\text{(inc)}} = -b_{J,-1}^{\text{(inc)}} = -i, \alpha^{(2)} = -\beta^{(2)} = i/k^{(2)}.$$

Similarly, the magnetic fields have the following expansion

$$c\mathbf{B}_{(1)} = \frac{1}{2} \sum_{J,M} C_J \left[\left\{ \beta^{(1)} \mathbf{a}_{J,M}^{(1)} \frac{i}{r} \frac{d[rj_J^{(1)}]}{dr} \right\} \mathbf{Y}_{J,M}^{(1)} + \left\{ \mathbf{b}_{J,M}^{(1)} j_J^{(1)} \right\} \mathbf{Y}_{J,M}^{(0)} + \left\{ \beta^{(1)} \mathbf{a}_{J,M}^{(1)} i \sqrt{J(J+1)} \frac{j_J^{(1)}}{r} \right\} \mathbf{Y}_{J,M}^{(-1)} \right], \quad (3.6)$$

$$c\mathbf{B}_{\text{(inc)}} = \frac{1}{2} \sum_{J,M} C_J \left[\left\{ \beta^{(2)} \mathbf{a}_{J,M}^{\text{(inc)}} \frac{i}{r} \frac{d[rj_J^{(2)}]}{dr} \right\} \mathbf{Y}_{J,M}^{(1)} + \left\{ \mathbf{b}_{J,M}^{\text{(inc)}} j_J^{(2)} \right\} \mathbf{Y}_{J,M}^{(0)} + \left\{ \beta^{(2)} \mathbf{a}_{J,M}^{\text{(inc)}} i \sqrt{J(J+1)} \frac{j_J^{(2)}}{r} \right\} \mathbf{Y}_{J,M}^{(-1)} \right], \quad (3.7)$$

$$c\mathbf{B}_{\text{(sc)}} = \frac{1}{2} \sum_{J,M} C_J \left[\left\{ \beta^{(2)} \mathbf{a}_{J,M}^{(\text{sc})} \frac{i}{r} \frac{d[rh_J^{(2)}]}{dr} \right\} \mathbf{Y}_{J,M}^{(1)} + \left\{ \mathbf{b}_{J,M}^{(\text{sc})} h_J^{(2)} \right\} \mathbf{Y}_{J,M}^{(0)} + \left\{ \beta^{(2)} \mathbf{a}_{J,M}^{(\text{sc})} i \sqrt{J(J+1)} \frac{h_J^{(2)}}{r} \right\} \mathbf{Y}_{J,M}^{(-1)} \right]. \quad (3.8)$$

Using the above expressions, the task of determining electromagnetic fields both spatially and temporally is simplified to discussing how the coefficients of these fields evolve over time. For this, we need a suitable model to describe the materials involved, that is, the metal and the dielectric medium with gain.

4 Free Electron Model

The free electron model for the metallic sphere describes the interaction of the electrons in the metal with the internal electric field:

$$\frac{d^2\mathbf{r}}{dt^2} + 2\gamma \frac{d\mathbf{r}}{dt} = \frac{e}{m_e} \mathbf{E}_{(1)}, \quad (4.1)$$

where \mathbf{r} represents the displacement of the electronic cloud within the metal (with respect to an equilibrium position), γ is the collisions friction coefficient, and e and m_e are the charge and mass of the electron.

A term $\Pi_{(1)}$ in the polarization of the metal can be attributed to the dislocation of electrical charges; $\Pi_{(1)} = n_e e \mathbf{r}$, where n_e is the number density of electrons in the metal:

$$\left(\frac{d^2}{dt^2} + 2\gamma \frac{d}{dt} \right) \Pi_{(1)} = \frac{n_e e^2}{m_e} \mathbf{E}_{(1)}. \quad (4.2)$$

Using the rotating wave approximation, $\Pi_{(1)} \rightarrow \Pi_{(1)} e^{-i\omega t}$ and $\mathbf{E}_{(1)} \rightarrow \mathbf{E}_{(1)} e^{-i\omega t}$, and discarding nonlinear time derivatives, we get

$$\frac{d\Pi_{(1)}}{dt} - \frac{\omega^2 + 2i\gamma\omega}{2(\gamma - i\omega)} \Pi_{(1)} = \frac{\varepsilon_0 \omega_{\text{pl}}^2}{2(\gamma - i\omega)} \mathbf{E}_{(1)}, \quad (4.3)$$

where ω_{pl} is the plasma frequency. In this work, we will study a silver nanosphere, for which $\hbar\omega_{\text{pl}} = 9.6$ [eV] and $\hbar\gamma = 0.0228$ [eV].

The free electron model imposes two conditions on the coefficients of the fields:

$$\frac{d\mathcal{D}_{J,M}^{(1)}}{dt} - \frac{\omega^2 + 2i\gamma\omega}{2(\gamma - i\omega)} \mathcal{D}_{J,M}^{(1)} - \frac{\varepsilon_0 \omega_{\text{pl}}^2}{2(\gamma - i\omega)} \mathcal{B}_{J,M}^{(1)} = 0, \quad (4.4)$$

$$\frac{d\mathbf{c}_{J,M}^{(1)}}{dt} - \frac{\omega^2 + 2i\gamma\omega}{2(\gamma - i\omega)} \mathbf{c}_{J,M}^{(1)} - \frac{\varepsilon_0\omega_{\text{pl}}^2}{2(\gamma - i\omega)} \mathbf{a}_{J,M}^{(1)} = 0. \quad (4.5)$$

To term $\mathbf{\Pi}_{(1)}$ must be added the contribution to metal polarization due to the ionic lattice. For this reason, we write the total polarization of the metal $\mathbf{P}_{(1)}$ as:

$$\mathbf{P}_{(1)} = \varepsilon_0\chi_\infty \mathbf{E}_{(1)} + \mathbf{\Pi}_{(1)}. \quad (4.6)$$

The electric displacement field within the metallic sphere $\mathbf{D}_{(1)}$ is

$$\mathbf{D}_{(1)} = \varepsilon_0 \mathbf{E}_{(1)} + \mathbf{P}_{(1)} = \varepsilon_\infty \mathbf{E}_{(1)} + \mathbf{\Pi}_{(1)}. \quad (4.7)$$

Using the same expansion as before,

$$\begin{aligned} \mathbf{\Pi}_{(1)} = \frac{1}{2} \sum_{J,M} C_J & \left[\left\{ \alpha^{(1)} \mathbf{d}_{J,M}^{(1)} \frac{i}{r} \frac{d[r j_J^{(1)}]}{dr} \right\} \mathbf{Y}_{J,M}^{(1)} + \left\{ \mathbf{c}_{J,M}^{(1)} j_J^{(1)} \right\} \mathbf{Y}_{J,M}^{(0)} + \right. \\ & \left. \left\{ \alpha^{(1)} \mathbf{d}_{J,M}^{(1)} i \sqrt{J(J+1)} \frac{j_J^{(1)}}{r} \right\} \mathbf{Y}_{J,M}^{(-1)} \right]. \end{aligned} \quad (4.8)$$

In a steady state, the derivative with respect to time in equation 4.3 is 0, so that the permittivity of the metal can be described as

$$\varepsilon_{(1)} = \varepsilon_\infty - \frac{\varepsilon_0\omega_{\text{pl}}^2}{\omega^2 + 2i\gamma\omega}, \quad (4.9)$$

which is predicted by the Drude model.

5 Optical Bloch Equations

In this section, we will study how the external field $\mathbf{E}_{(2)}$ interacts with the gain medium. This is a purely quantum interaction, which is described as a two-state quantum system by the optical Bloch equations and the quantum formalism of the density matrix [11]:

$$\frac{d\rho_{12}}{dt} - \left(i\omega_{21} - \frac{1}{\tau_2} \right) \rho_{21} = \frac{iN\boldsymbol{\mu} \cdot \mathbf{E}_{(2)}}{\hbar}, \quad (5.1)$$

$$\frac{dN}{dt} + \frac{N - \tilde{N}}{\tau_1} = \frac{2i(\rho_{12} - \rho_{21})\boldsymbol{\mu} \cdot \mathbf{E}_{(2)}}{\hbar}. \quad (5.2)$$

ρ_{ij} is the i,j element of the density matrix; $\tau_1^{-1} = \tilde{\tau}_1^{-1} + W$ is an effective relaxation rate, with W being a phenomenological pumping rate; $\tilde{\tau}_1$ and τ_2 are time constants associated with spontaneous energy emission and phase relaxation processes due to interaction with the environment; $\omega_{21} = (E_2 - E_1)/\hbar$ is the transition frequency between levels 1 and 2; $N = \rho_{22} - \rho_{11}$ is the population inversion, with ρ_{11} and ρ_2 being the diagonal elements of the density matrix; $\boldsymbol{\mu}$ is the transition dipole moment of the active elements; and $\tilde{N} = (W\tilde{\tau}_1 - 1)/(W\tilde{\tau}_1 + 1)$ is the population inversion due to the pump (in the absence of the pump, we have $\tilde{N} = -1$). $\tilde{N} > 0$ corresponds to the regime of amplification; $\tilde{N} < 0$ to losses.

Let χ_b be the susceptibility of the dielectric host and n the numerical density of the active elements, then the polarization outside the nanosphere $\mathbf{P}_{(2)}$ is obtained by averaging the dipole moments of the gain elements, assuming that these are oriented randomly with respect to the $\mathbf{E}_{(2)}$ field:

$$\mathbf{P}_{(2)} = \varepsilon_0 \chi_b \mathbf{E}_{(2)} + \frac{n}{4\pi} \int_{\Omega} (\rho_{12} + \rho_{21}) \boldsymbol{\mu} d\Omega = \varepsilon_0 \chi_b \mathbf{E}_{(2)} + 2\Re[\mathbf{\Pi}_{(2)}], \quad (5.3)$$

where Ω is the solid angle and

$$\Pi_{(2)} = \frac{n}{4\pi} \int_{\Omega} \rho_{12} \mu d\Omega \quad (5.4)$$

is the term of the polarization contributed by the emitters.

Next, we use the rotating wave approximation again, assuming that the frequency of the probe field $\mathbf{E}_{(\text{inc})}$ is nearly resonant ($\omega \approx \omega_{21}$) and that all time-dependent fields assume a harmonic form $e^{-i\omega t}$. With this approximation, the resulting equations are [8]:

$$\mathbf{P}_{(2)} = \varepsilon_0 \chi_b \mathbf{E}_{(2)} + 2\Pi_{(2)}, \quad (5.5)$$

$$\frac{d\Pi_{(2)}}{dt} + \left[\frac{1}{\tau_2} - i(\omega - \omega_{21}) \right] \Pi_{(2)} = \frac{i\varepsilon_0 NG}{2\tau_2 \tilde{N}} \mathbf{E}_{(2)}, \quad (5.6)$$

$$\frac{dN}{dt} + \frac{N - \tilde{N}}{\tau_1} = -\frac{2}{n\hbar} \Im(\mathbf{E}_{(2)} \cdot \Pi_{(2)}^*), \quad (5.7)$$

where

$$G \equiv -\frac{n\mu^2 \tau_2 \tilde{N}}{3\hbar\varepsilon_0}$$

is a (negative) quantity that will describe the level of gain. The quantity G will be used extensively to characterize the different operational ranges that the system under study has.

Using our expansion, we write the nonlinear term of polarization in the external medium as

$$\begin{aligned} \mathbf{\Pi}_{(2)} = & \frac{1}{2} \sum_{J,M} C_J \left[\left\{ \alpha^{(2)} \mathbf{d}_{J,M}^{(2)} \frac{i}{r} \frac{d[r h_J^{(2)}]}{dr} \right\} \mathbf{Y}_{J,M}^{(1)} + \left\{ \mathbf{c}_{J,M}^{(2)} h_J^{(2)} \right\} \mathbf{Y}_{J,M}^{(0)} + \right. \\ & \left. \left\{ \alpha^{(2)} \mathbf{d}_{J,M}^{(2)} i \sqrt{J(J+1)} \frac{h_J^{(2)}}{r} \right\} \mathbf{Y}_{J,M}^{(-1)} \right]. \end{aligned} \quad (5.8)$$

Then, the electric displacement field in the external medium $\mathbf{D}_{(2)}$ assumes the following form

$$\mathbf{D}_{(2)} = \varepsilon_0 \mathbf{E}_{(2)} + \mathbf{P}_{(2)} = \varepsilon_b \mathbf{E}_{(2)} + 2\mathbf{\Pi}_{(2)}, \quad (5.9)$$

where $\varepsilon_b = \varepsilon_0 (1 + \chi_b)$ is the permittivity of the dielectric host.

The first optical Bloch equation, eq. 5.6, imposes two additional conditions on the coefficients:

$$h_J^{(2)} \frac{dc_{J,M}^{(2)}}{dt} + h_J^{(2)} \left[\frac{1}{\tau_2} - i(\omega - \omega_{21}) \right] c_{J,M}^{(2)} - \frac{i\varepsilon_0 G N}{2\tau_2 \tilde{N}} \left[j_J^{(2)} \mathbf{a}_{J,M}^{(\text{inc})} + h_J^{(2)} \mathbf{a}_{J,M}^{(\text{sc})} \right] = 0, \quad (5.10)$$

$$h_J^{(2)} \frac{dd_{J,M}^{(2)}}{dt} + h_J^{(2)} \left[\frac{1}{\tau_2} - i(\omega - \omega_{21}) \right] d_{J,M}^{(2)} - \frac{i\varepsilon_0 G N}{2\tau_2 \tilde{N}} \left[j_J^{(2)} \mathbf{b}_{J,M}^{(\text{inc})} + h_J^{(2)} \mathbf{b}_{J,M}^{(\text{sc})} \right] = 0. \quad (5.11)$$

For the second Bloch equation, eq. 5.7, we will need to handle the following product numerically:

$$\begin{aligned}
& \mathbf{E}_{(2)} \cdot \boldsymbol{\Pi}_{(2)}^* = \\
& \frac{1}{4} \sum_{J_1, M_1, J_2, M_2} C_{J_1} C_{J_2}^* \\
& \left[\frac{|\alpha^{(2)}|^2}{r^2} \left\{ b_{J_1, M_1}^{(\text{inc})} \frac{d[rj_{J_1}^{(2)}]}{dr} + b_{J_1, M_1}^{(\text{sc})} \frac{d[rh_{J_1}^{(2)}]}{dr} \right\} d_{J_2, M_2}^{(2)*} \frac{d[rh_{J_2}^{(2)}]}{dr}^* \mathbf{Y}_{J_1, M_1}^{(1)} \cdot \mathbf{Y}_{J_2, M_2}^{(1)*} \right. \\
& + \frac{i}{r} \alpha^{(2)} \left\{ b_{J_1, M_1}^{(\text{inc})} \frac{d[rj_{J_1}^{(2)}]}{dr} + b_{J_1, M_1}^{(\text{sc})} \frac{d[rh_{J_1}^{(2)}]}{dr} \right\} c_{J_2, M_2}^{(2)*} h_{J_2}^{(2)*} \mathbf{Y}_{J_1, M_1}^{(1)} \cdot \mathbf{Y}_{J_2, M_2}^{(0)*} \\
& - \frac{i}{r} \alpha^{(2)*} \left\{ a_{J_1, M_1}^{(\text{inc})} j_{J_1}^{(2)} + a_{J_1, M_1}^{(\text{sc})} h_{J_1}^{(2)} \right\} d_{J_2, M_2}^{(2)*} \frac{d[rh_{J_2}^{(2)}]}{dr}^* \mathbf{Y}_{J_1, M_1}^{(0)} \cdot \mathbf{Y}_{J_2, M_2}^{(1)*} \\
& + \left\{ a_{J_1, M_1}^{(\text{inc})} j_{J_1}^{(2)} + a_{J_1, M_1}^{(\text{sc})} h_{J_1}^{(2)} \right\} c_{J_2, M_2}^{(2)*} h_{J_2}^{(2)*} \mathbf{Y}_{J_1, M_1}^{(0)} \cdot \mathbf{Y}_{J_2, M_2}^{(0)*} \\
& \left. + \frac{|\alpha^{(2)}|^2}{r^2} \sqrt{J_1(J_1+1)J_2(J_2+1)} \left\{ b_{J_1, M_1}^{(\text{inc})} j_{J_1}^{(2)} + b_{J_1, M_1}^{(\text{sc})} h_{J_1}^{(2)} \right\} d_{J_2, M_2}^{(2)*} h_{J_2}^{(2)*} \mathbf{Y}_{J_1, M_1}^{(-1)} \cdot \mathbf{Y}_{J_2, M_2}^{(-1)*} \right] \quad (5.12)
\end{aligned}$$

Assuming that the system reaches a steady state, the derivatives with respect to time in equations 5.6 and 5.7 are null, with which we obtain the following relationships:

$$2\boldsymbol{\Pi}_{(2)} = -\frac{N}{\tilde{N}} \frac{\varepsilon_0 G \Delta}{2(\omega - \omega_{21}) + i\Delta} \mathbf{E}_{(2)}, \quad (5.13)$$

$$N = \tilde{N} \frac{4(\omega - \omega_{21})^2 + \Delta^2}{4(\omega - \omega_{21})^2 + \Delta^2 \left[1 + \left(\frac{|\mathbf{E}_{(2)}|}{E_{\text{sat}}} \right)^2 \right]}, \quad (5.14)$$

where the saturation field is defined as

$$E_{\text{sat}} = \sqrt{\frac{3}{\tau_1 \tau_2}} \frac{\hbar}{\mu}.$$

Then the relation $D = \varepsilon_{(2)}E$ implies that the permittivity of the gain medium is

$$\begin{aligned}\varepsilon_{(2)} &= \varepsilon_b - \varepsilon_0 G \Delta \frac{2(\omega - \omega_{21}) - i\Delta}{4(\omega - \omega_{21})^2 + \Delta^2 \left[1 + \left(\frac{|\mathbf{E}_{(2)}|}{E_{\text{sat}}} \right)^2 \right]} \\ &\approx \varepsilon_b - \frac{\varepsilon_0 G \Delta}{2(\omega - \omega_{21}) + i\Delta},\end{aligned}\quad (5.15)$$

where the approximation is valid when $N \approx \tilde{N}$ (this will happen for small values of G in the linear amplification regime).

6 Boundary Conditions

In the previous sections, we modeled the differential equations that describe the time dependence of the fields in the metal and in the surrounding medium. These equations are coupled by the boundary conditions. If \mathbf{n} is a vector normal to the surface of the sphere, then the boundary conditions, which establish the tangential and normal continuity of the fields on the surface of the nanosphere, are written as

$$\mathbf{n} \times (\mathbf{E}_{(\text{sc})} + \mathbf{E}_{(\text{inc})} - \mathbf{E}_{(1)}) = \mathbf{0}, \quad (6.1)$$

$$\mathbf{n} \cdot (\mathbf{D}_{(2)} - \mathbf{D}_{(1)}) = 0, \quad (6.2)$$

$$\mathbf{n} \times (\mathbf{B}_{(\text{sc})} + \mathbf{B}_{(\text{inc})} - \mathbf{B}_{(1)}) = \mathbf{0}, \quad (6.3)$$

$$\mathbf{n} \cdot (\mathbf{B}_{(\text{sc})} + \mathbf{B}_{(\text{inc})} - \mathbf{B}_{(1)}) = 0. \quad (6.4)$$

Here we consider that the magnetic permeability of the particle and the surrounding medium is the same. Equations 6.1-6.4 would impose $\beta^{(1)} = \beta^{(2)}$, and the following restrictions on the coefficients of the fields:

$$b_{J,M}^{(sc)} \frac{d[rh_J^{(2)}]}{dr} \Big|_{r=a} + b_{J,M}^{(inc)} \frac{d[rj_J^{(2)}]}{dr} \Big|_{r=a} = \frac{\alpha^{(1)}}{\alpha^{(2)}} b_{J,M}^{(1)} \frac{d[rj_J^{(1)}]}{dr} \Big|_{r=a}, \quad (6.5)$$

$$\begin{aligned} \varepsilon_b \left(b_{J,M}^{(inc)} j_J^{(2)} \Big|_{r=a} + b_{J,M}^{(sc)} h_J^{(2)} \Big|_{r=a} \right) + 2d_{J,M}^{(2)} h_J^{(2)} \Big|_{r=a} = \\ \frac{\alpha^{(1)}}{\alpha^{(2)}} \left[\varepsilon_\infty b_{J,M}^{(1)} j_J^{(1)} \Big|_{r=a} + d_{J,M}^{(1)} j_J^{(1)} \Big|_{r=a} \right], \end{aligned} \quad (6.6)$$

$$a_{J,M}^{(sc)} h_J^{(2)} \Big|_{r=a} + a_{J,M}^{(inc)} j_J^{(2)} \Big|_{r=a} = a_{J,M}^{(1)} j_J^{(1)} \Big|_{r=a}, \quad (6.7)$$

$$a_{J,M}^{(sc)} \frac{d[rh_J^{(2)}]}{dr} \Big|_{r=a} + a_{J,M}^{(inc)} \frac{d[rj_J^{(2)}]}{dr} \Big|_{r=a} = a_{J,M}^{(1)} \frac{d[rj_J^{(1)}]}{dr} \Big|_{r=a}, \quad (6.8)$$

where the functions are evaluated on the surface of the nanoparticle, $r = a$.

Equations 6.7 and 6.8 can be rewritten to determine the coefficients $a_{J,M}^{(sc)}$ and $a_{J,M}^{(1)}$ in terms of $a_{J,M}^{(inc)}$ as:

$$a_{J,M}^{(sc)} = a_{J,M}^{(inc)} \frac{j_J^{(1)} \frac{d[rj_J^{(2)}]}{dr} - j_J^{(2)} \frac{d[rj_J^{(1)}]}{dr}}{h_J^{(2)} \frac{d[rj_J^{(1)}]}{dr} - j_J^{(1)} \frac{d[rh_J^{(2)}]}{dr}} \Big|_{r=a}, \quad (6.9)$$

$$a_{J,M}^{(1)} = a_{J,M}^{(inc)} \frac{j_J^{(2)} \frac{d[rh_J^{(2)}]}{dr} - h_J^{(2)} \frac{d[rj_J^{(2)}]}{dr}}{j_J^{(1)} \frac{d[rh_J^{(2)}]}{dr} - h_J^{(2)} \frac{d[rj_J^{(1)}]}{dr}} \Big|_{r=a}. \quad (6.10)$$

If for a moment we ignore the coefficient $d_{J,M}^{(2)}$, which correspond to the non-linear term of polarization in the outer media, and we write the result in the steady state for $d_{J,M}^{(1)}$, then the coefficients $a_{J,M}^{(sc)}$ and $a_{J,M}^{(1)}$ can also be determined in terms of the incident field as:

$$b_{J,M}^{(sc)} = b_{J,M}^{(inc)} \frac{j_J^{(2)} \frac{d[rj_J^{(1)}]}{dr} - m^2 j_J^{(1)} \frac{d[rj_J^{(2)}]}{dr}}{m^2 j_J^{(1)} \frac{d[rh_J^{(2)}]}{dr} - h_J^{(2)} \frac{d[rj_J^{(1)}]}{dr}} \Big|_{r=a}, \quad (6.11)$$

$$b_{J,M}^{(1)} = b_{J,M}^{(inc)} \frac{\alpha^{(2)}}{\alpha^{(1)}} \frac{j_J^{(2)} \frac{d[rh_J^{(2)}]}{dr} - h_J^{(2)} \frac{d[rj_J^{(2)}]}{dr}}{m^2 j_J^{(1)} \frac{d[rh_J^{(2)}]}{dr} - h_J^{(2)} \frac{d[rj_J^{(1)}]}{dr}} \Big|_{r=a}, \quad (6.12)$$

where

$$m^2 = \frac{\varepsilon_\infty - \frac{\varepsilon_0 \omega_{pl}^2}{\omega^2 + 2i\gamma\omega}}{\varepsilon_b}.$$

If we let $\alpha^{(2)}/\alpha^{(1)} = m$, then equations 6.9-6.12 together are the coefficients that describe the fields calculated with Mie theory.

7 Numerical Resolution of Equations

The equations of the free electron model 4.1-4.2, the Bloch equations 5.7 and 5.10-5.11, and the boundary conditions 6.5-6.6 and 6.9-6.10 that describe the plasmonic response of the metallic nanosphere will be solved using computational methods. These differential equations are coupled and non-linear, so their solution cannot generally be found analytically. For this purpose, it is necessary to rewrite the equations so that they can be handled more easily by a computer.

The following coefficients are defined

$$C_1 = \textcolor{red}{b}_{J,M}^{(\text{inc})} \varepsilon_b \left(j_J^{(2)} - h_J^{(2)} \frac{\frac{d}{dr} \left[rj_J^{(2)} \right]}{\frac{d}{dr} \left[rh_J^{(2)} \right]} \right), \quad (7.1)$$

$$C_2 = \varepsilon_b h_J^{(2)} \frac{\frac{d}{dr} \left[rj_J^{(1)} \right]}{\frac{d}{dr} \left[rh_J^{(2)} \right]} - \varepsilon_\infty j_J^{(1)}, \quad (7.2)$$

$$C_3 = \frac{i\varepsilon_0 G N}{2\tau_2 \tilde{N}}. \quad (7.3)$$

We start by rewriting equation 6.5 as:

$$b_{J,M}^{(\text{sc})} = \frac{\frac{\alpha^{(1)}}{\alpha^{(2)}} \textcolor{blue}{b}_{J,M}^{(1)} \frac{d}{dr} \left[rj_J^{(1)} \right] \Big|_{r=a} - \textcolor{red}{b}_{J,M}^{(\text{inc})} \frac{d}{dr} \left[rj_J^{(2)} \right] \Big|_{r=a}}{\frac{d}{dr} \left[rh_J^{(2)} \right] \Big|_{r=a}}. \quad (7.4)$$

Substituting 7.4 into 6.6, we get

$$\textcolor{blue}{b}_{J,M}^{(1)} = \frac{\textcolor{violet}{d}_{J,M}^{(1)} j_J^{(1)} - 2m \textcolor{brown}{d}_{J,M}^{(2)} h_J^{(2)} - m C_1}{C_2}. \quad (7.5)$$

In turn, using equation 7.5, the differential equations 4.1 and 5.11 are rewritten as

$$\frac{d \textcolor{violet}{d}_{J,M}^{(1)}}{dt} - \frac{\omega^2 + 2i\gamma\omega + \varepsilon_0 \omega_{\text{pl}}^2 \frac{j_J^{(1)}}{C_2}}{2(\gamma - i\omega)} \textcolor{violet}{d}_{J,M}^{(1)} + \frac{\varepsilon_0 m \omega_{\text{pl}}^2 h_J^{(2)}}{C_2(\gamma - i\omega)} \textcolor{brown}{d}_{J,M}^{(2)} + \frac{\varepsilon_0 \omega_{\text{pl}}^2 m C_1}{2C_2(\gamma - i\omega)} = 0, \quad (7.6)$$

$$\frac{d\mathbf{d}_{J,M}^{(2)}}{dt} + \left(\begin{array}{c} 2C_3 h_J^{(2)} \frac{d[rj_J^{(1)}]}{dr} \\ \frac{1}{\tau_2} - i(\omega - \omega_{21}) + \frac{C_2 \frac{d[rh_J^{(2)}]}{dr}}{C_2 \frac{d[rh_J^{(2)}]}{dr}} \end{array} \right) \mathbf{d}_{J,M}^{(2)} \\ - \frac{C_3 j_J^{(1)} \frac{d[rj_J^{(1)}]}{dr}}{mC_2 \frac{d[rh_J^{(2)}]}{dr}} \mathbf{d}_{J,M}^{(1)} + \frac{C_1 C_3}{h_J^{(2)}} \left(\begin{array}{c} \frac{d[rj_J^{(1)}]}{dr} \\ \frac{C_2 \frac{d[rh_J^{(2)}]}{dr}}{C_2 \frac{d[rh_J^{(2)}]}{dr}} - \frac{1}{\varepsilon_b} \end{array} \right) = 0. \quad (7.7)$$

The problem then boils down to solving the coupled equations 7.6-7.7.

The permittivities also change with the variations of the fields according to the following relation

$$\varepsilon_{(1)} = \varepsilon_\infty - \frac{\Pi_{(1)} \cdot \mathbf{E}_{(1)}^*}{|\mathbf{E}_{(1)}|^2}, \quad (7.8)$$

$$\varepsilon_{(2)} = \varepsilon_b - 2 \frac{\Pi_{(2)} \cdot \mathbf{E}_{(2)}^*}{|\mathbf{E}_{(2)}|^2}. \quad (7.9)$$

A metallic nanoparticle naturally possesses a dipole localized plasmon resonance frequency ω_0 , which can be calculated from the permitivities using the standard Fröhlich condition [12]:

$$\Re(\varepsilon_{(1)}(\omega_0) + 2\varepsilon_{(2)}(\omega_0)) = 0. \quad (7.10)$$

In all our characterizations, we have assumed that the emission line shape of the gain medium is centered exactly on the frequency of the plasmon. This means that $\omega_{21} = \omega_0$. In this way, a better coupling efficiency between the gain and the metal is expected. Under this assumption, condition

[7.10](#) is read as:

$$\omega_{21} = \sqrt{\frac{\varepsilon_0 \omega_{\text{pl}}^2}{\varepsilon_\infty + 2\varepsilon_b} - 4\gamma^2}. \quad (7.11)$$

8 Linear Amplification Regime

We start by considering scenarios in which the gain value G is very low and the system remains below a threshold in amplification. Here, we assume that the amplitudes of the probe $\mathbf{E}_{(\text{inc})}$ and the field $\mathbf{E}_{(2)}$ are small enough that the term on the right hand side of eq. [5.7](#) is negligible. This means that no field becomes extremely intense and the population investment is spatially uniform: $N(r, \theta, \phi, t) = \tilde{N}$. This has physically important implications: the system becomes linear and the dipole terms are the most prevalent. Because of these conditions, the higher order multipolar terms decay over time and become insignificant.

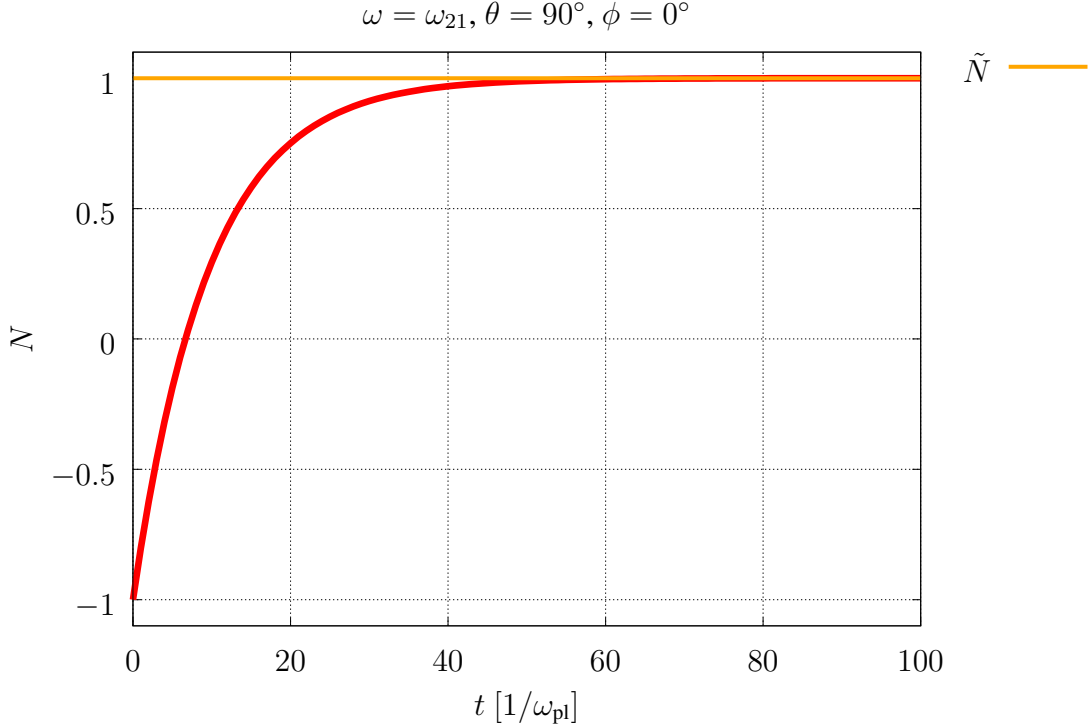


Figure 2: Temporal evolution of N for $G = -0.01$. Eventually, $N \approx \tilde{N}$ is obtained when the value of G is relatively small, without dependence on the θ and ϕ coordinates. We assume a large fixed power for the pump: $\tilde{N} = 1$.

When the plasmonic response is predominantly dipolar, we can study the polarizability of the system. The polarizability α of the nanoparticle is classically defined as

$$\alpha = 4\pi\varepsilon_0 a^3 \frac{\varepsilon_{(1)} - \varepsilon_{(2)}}{\varepsilon_{(1)} + 2\varepsilon_{(2)}}. \quad (8.1)$$

The evolution of polarizability is shown in Figure 3 for the same silver nanoparticle with a radius of 10 [nm], where the level of gain G is progressively increased from zero towards increasingly negative values. We have assumed again a large fixed power for the pump: $\tilde{N} = 1$.

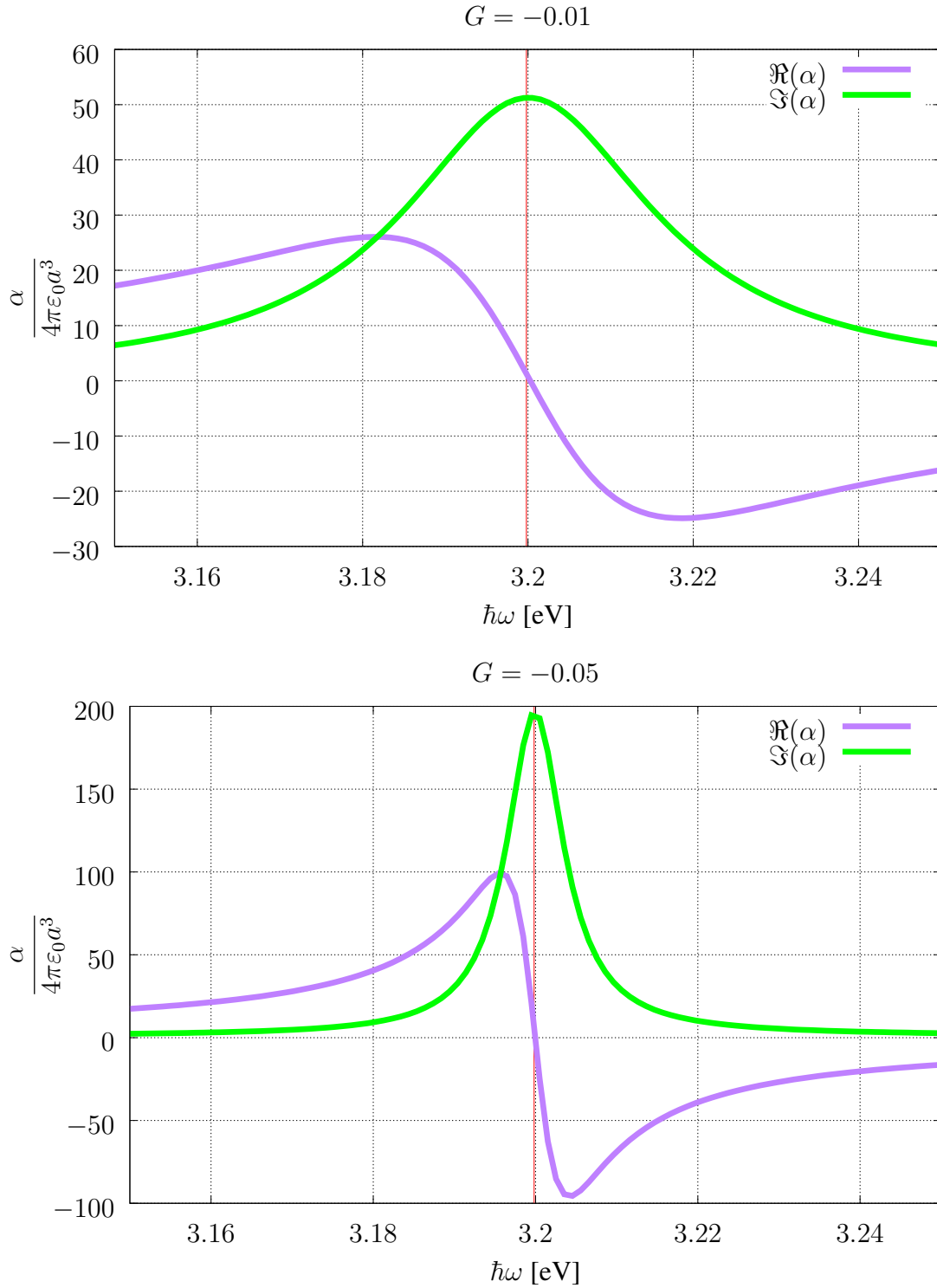


Figure 3: Plasmonic response of a 10 [nm] silver nanoparticle as gain is increased in the surrounding medium. Parameters: $\varepsilon_b = 1.8496\varepsilon_0$ (ethanol solvent), $\hbar\omega_{21} = 3.2$ [eV], $\Delta = 0.2$ [eV].

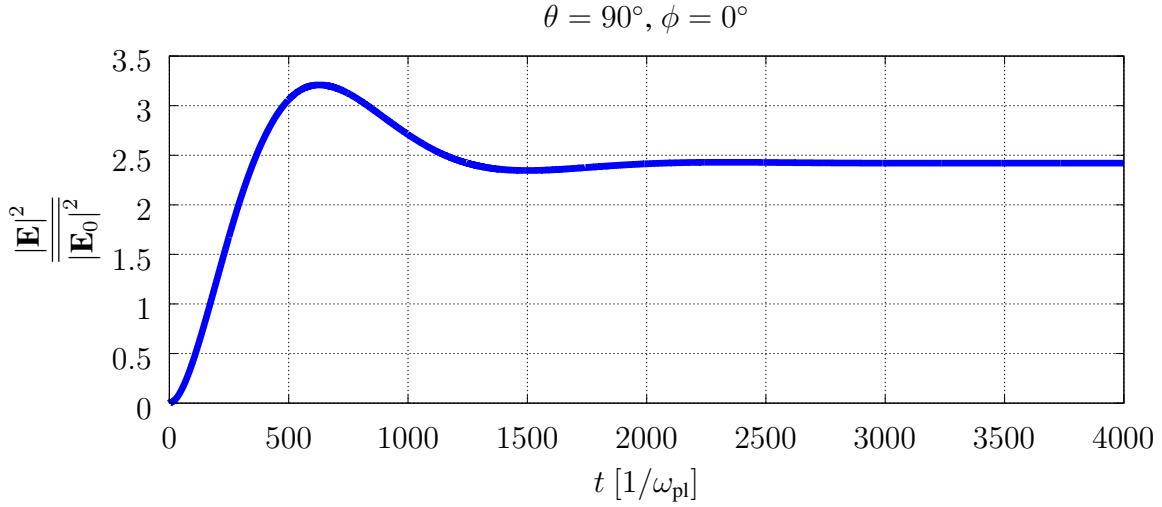


Figure 4: Time evolution of $|E|^2 / |E_0|^2$ at different points on the surface of the sphere when $G = -0.01$ and $\omega = \omega_{21}$. $\mathbf{E} = \mathbf{E}_{(2)}$ is the external electric field. $\overline{|E_0|^2}$ is the average of $|\mathbf{E}_{(2)}|^2$ on the surface of the sphere when $G = 0$.

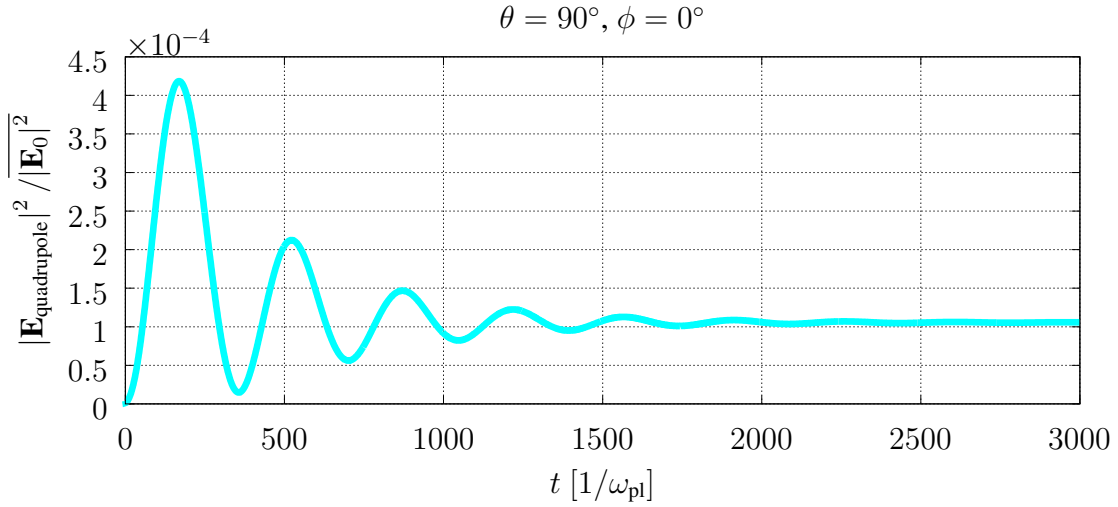


Figure 5: Time evolution of $|\mathbf{E}_{\text{quadrupole}}|^2 / |\mathbf{E}_0|^2$ at different points on the surface of the sphere when $G = -0.01$ and $\omega = \omega_{21}$. In $|\mathbf{E}_{\text{quadrupole}}|^2$ only the terms with $J = 2$ are taken into account during the calculation of the external electric field, which corresponds to the quadrupole term of the field.

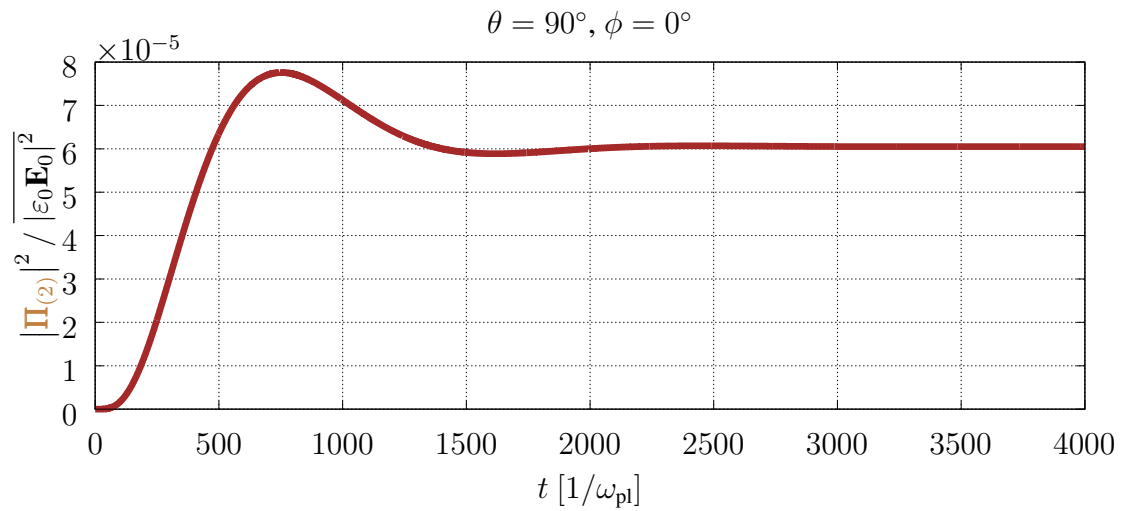


Figure 6: Time evolution of $\left| \Pi_{(2)} \right|^2 / \left| \varepsilon_0 \mathbf{E}_0 \right|^2$ when $G = -0.01$ and $\omega = \omega_{21}$.

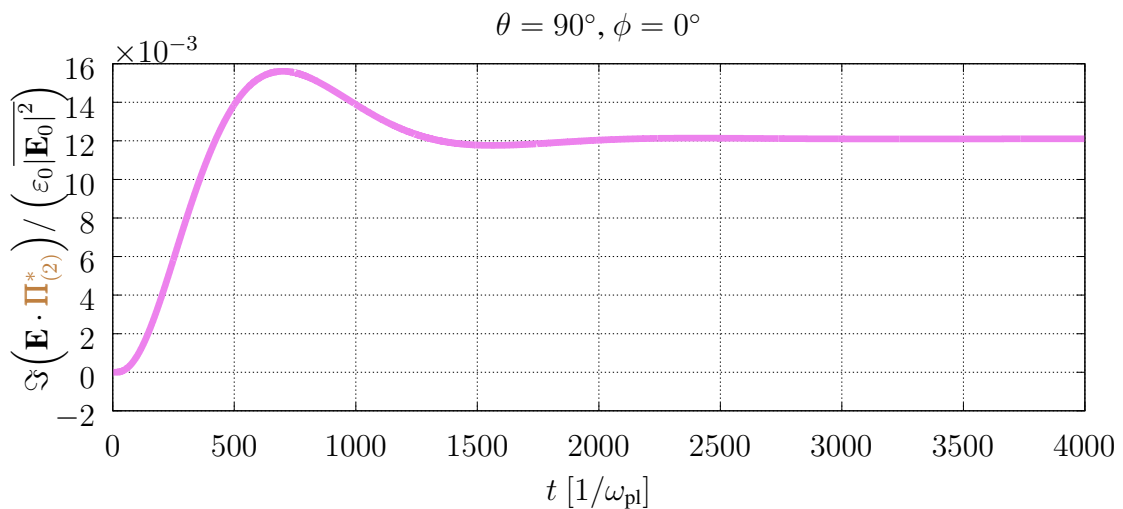


Figure 7: Time evolution of $\Im(\mathbf{E} \cdot \Pi_{(2)}^*) / \left(\varepsilon_0 \left| \mathbf{E}_0 \right|^2 \right)$ when $G = -0.01$ and $\omega = \omega_{21}$. $\mathbf{E} = \mathbf{E}_{(2)}$ is the external electric field.

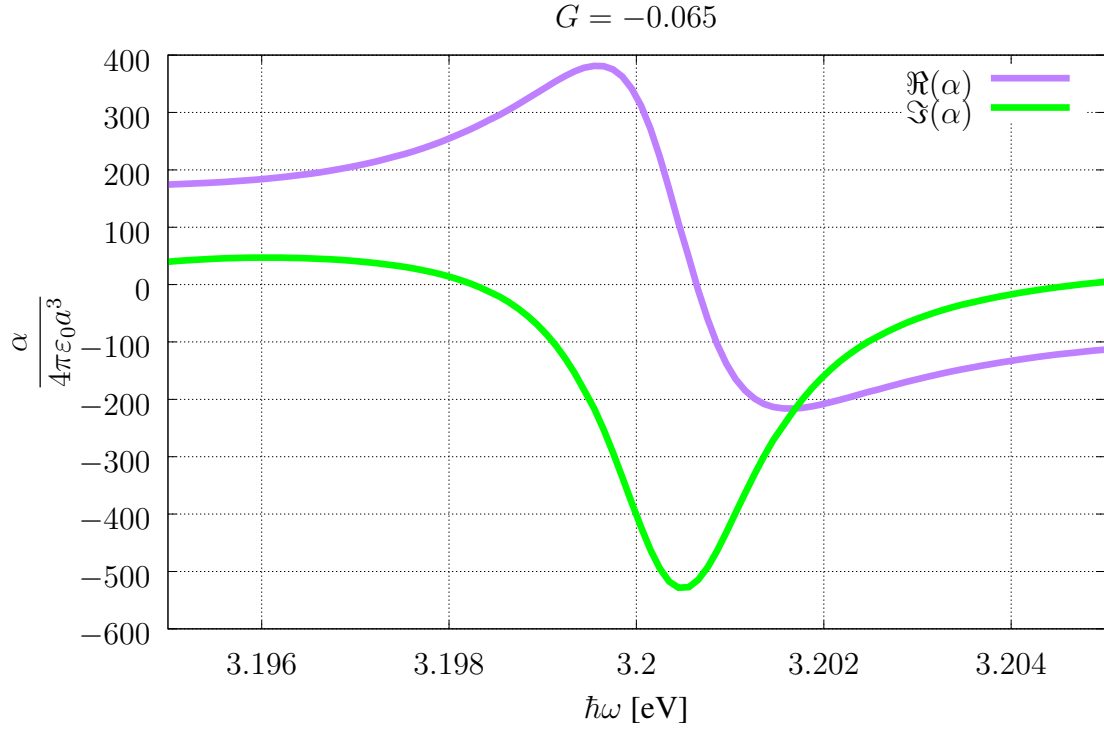


Figure 8: Plasmonic response for values of G for which the system goes into a nonlinear amplification regime. An easy rule of thumb to predict the extent of the linear amplification regime is to look for a sign change in the imaginary part of the polarizability (compare with Fig. 3) [8].

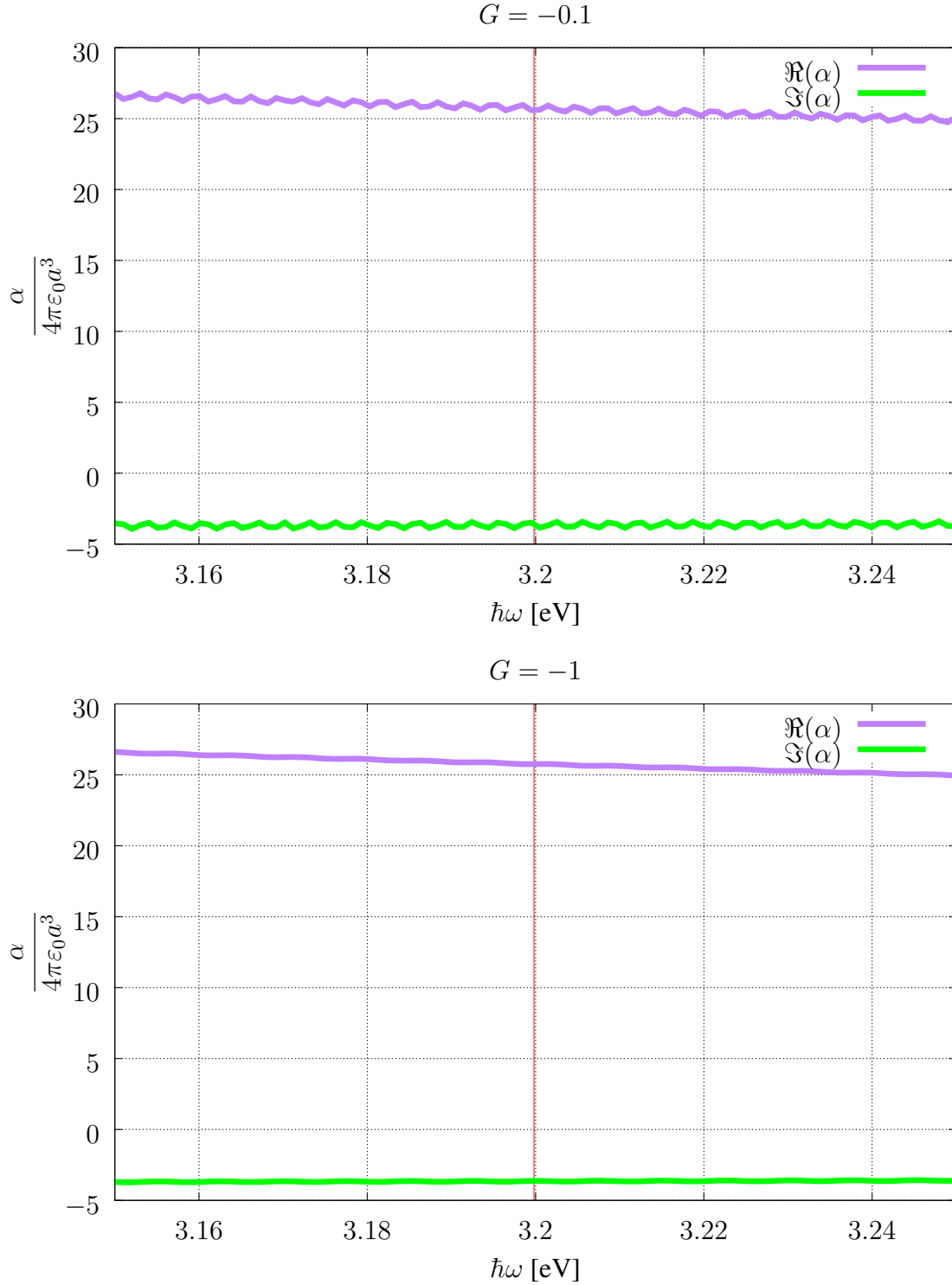


Figure 9: When the gain value exceeds a threshold and the system goes into a nonlinear regime, the dipolar approximation of the plasmonic response is no longer valid.

We observe that the plasmon (the resonance observed in polarizability) is gradually amplified and has increasing fineness for more negative values of G (see Fig. 3). This is in correspondence with the linear amplification regime, where a partial compensation of the loss occurs. This regime is ideal for applications because it requires relatively small gain values to be introduced into the dielectric host. Additionally, this system by itself is capable of compensating for intrinsic losses in plasmonic resonances.

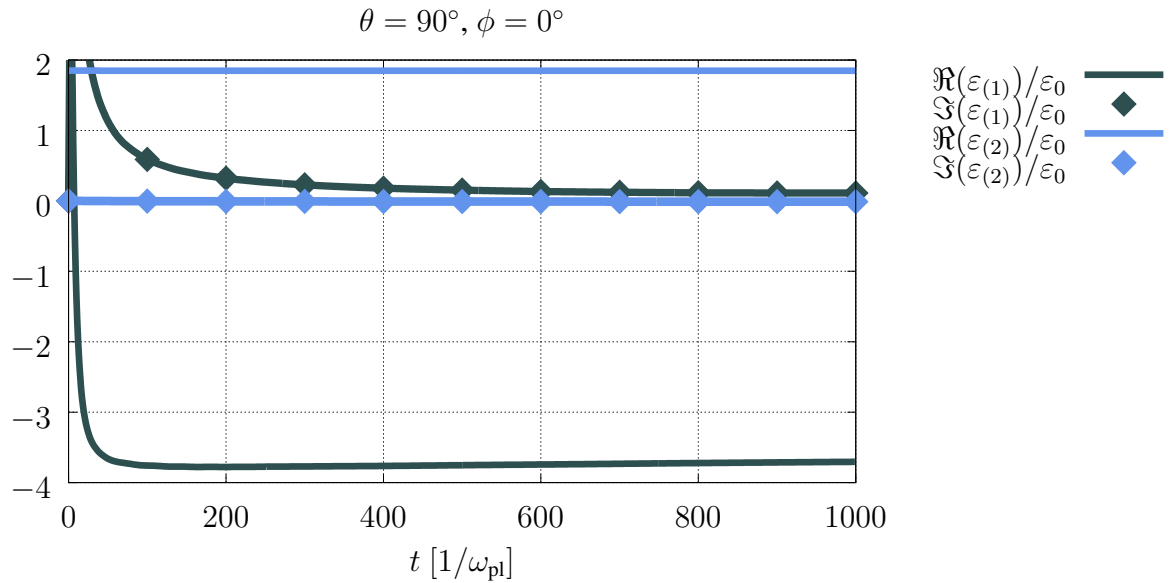


Figure 10: Evolution of the permittivities in the metal and the gain medium for $G = -0.01$ and $\omega = \omega_{21}$. The permitivities converge to the values given by equations 4.9 and 5.15.

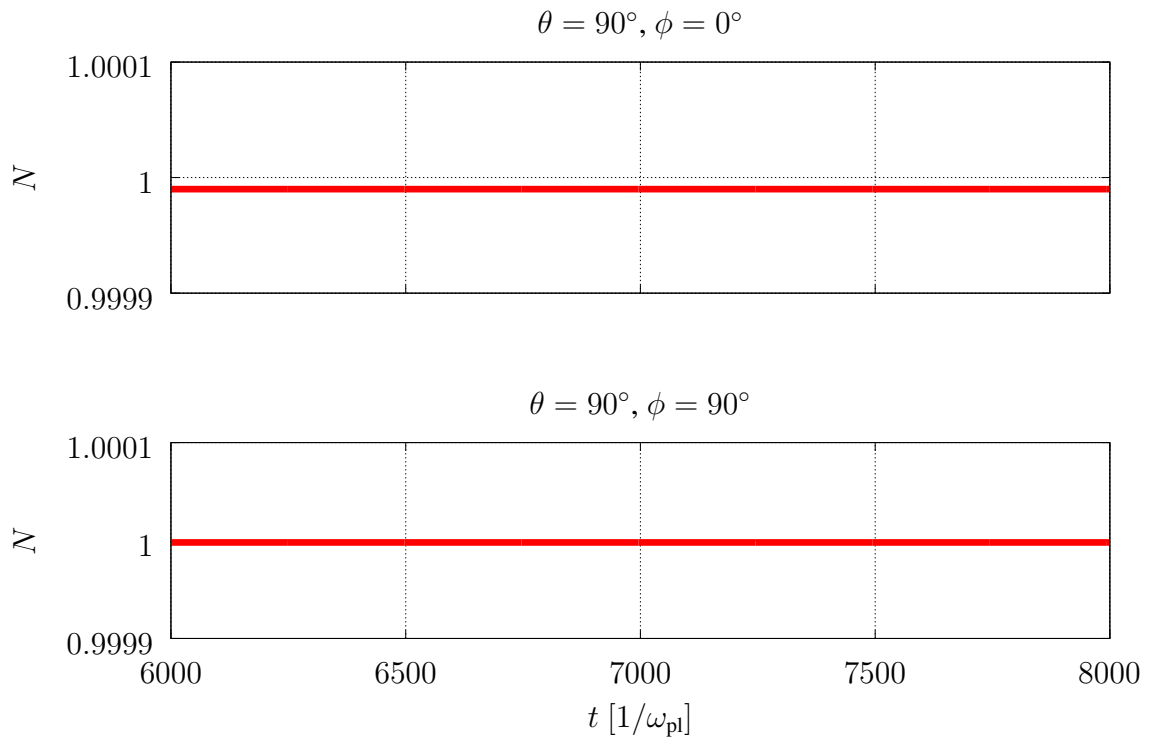


Figure 11: A close inspection of the temporal evolution of N , showing that it converges approximately to \tilde{N} . This result is shown at two points on the surface of the nanosphere.

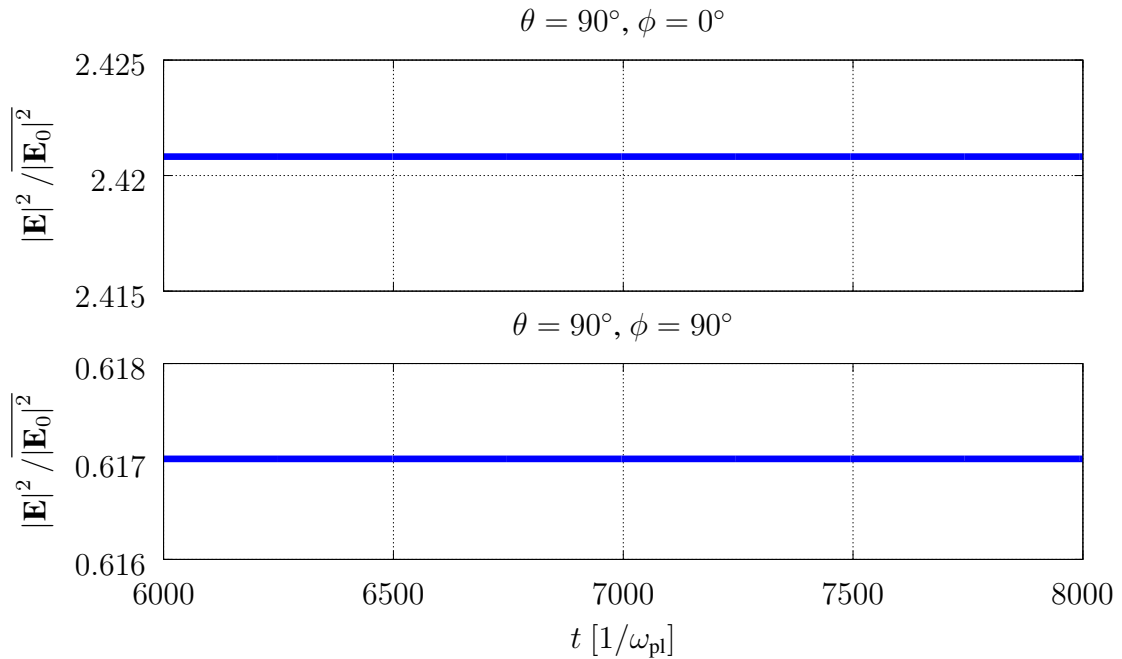


Figure 12: A close inspection of the temporal evolution of $|\mathbf{E}|^2$, showing that it converges. This result is shown at two points on the surface of the nanosphere. It is observed that the external electric field is more intense when $\theta = 90^\circ$ and $\phi = 0^\circ$, which corresponds to the pole of the nanosphere that is on the x -axis, the axis that has the same direction as the incident electric field.

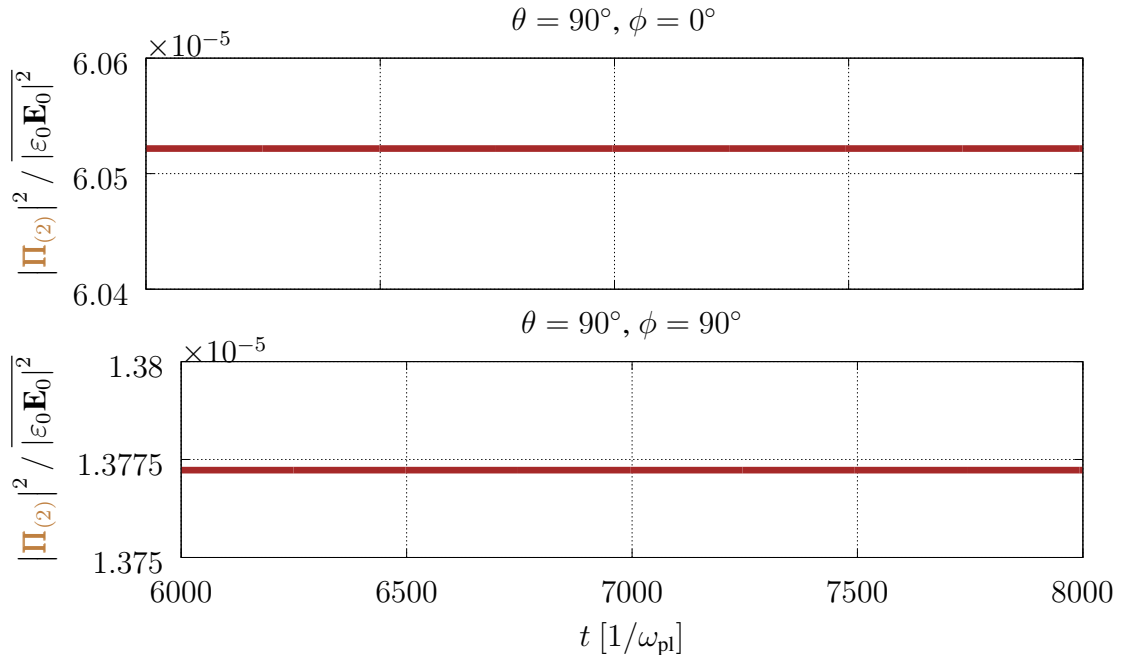


Figure 13: A close inspection of the temporal evolution of $|\Pi_{(2)}|^2$ shows that it converges.

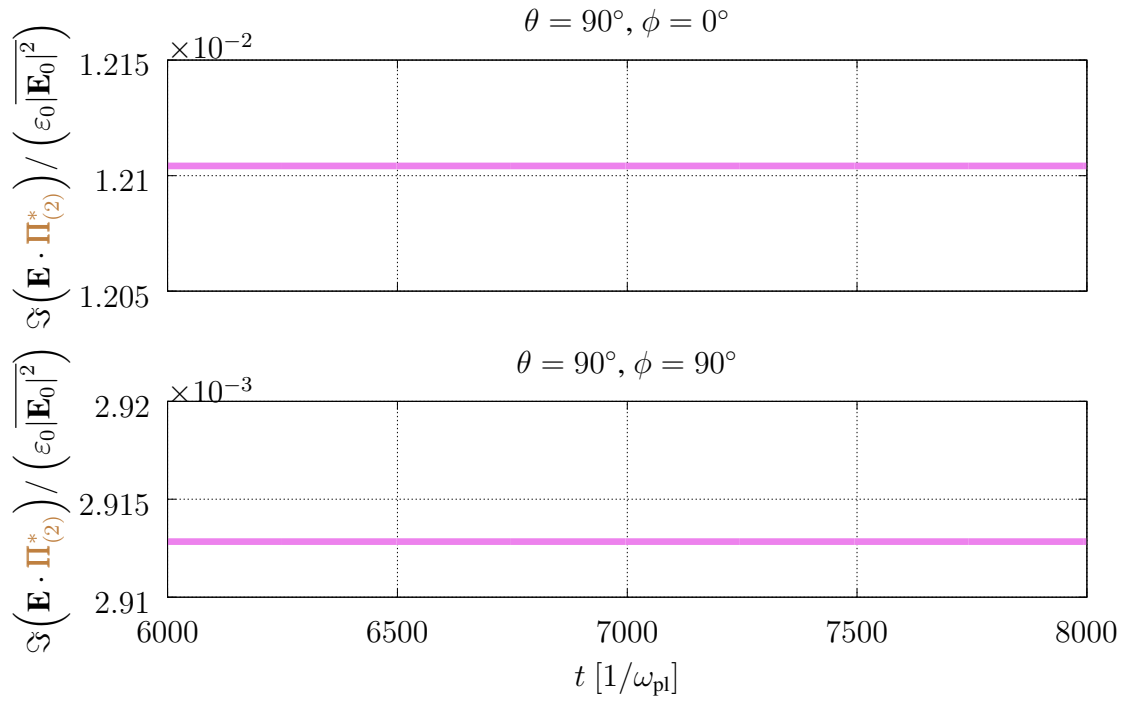


Figure 14: A close inspection of the temporal evolution of $\Im(\mathbf{E} \cdot \Pi_{(2)}^*) / (\varepsilon_0 |\mathbf{E}_0|^2)$ shows that it converges.

The relatively small magnitude of this quantity explains why N converges to values close to \tilde{N} , as indicated by equation 5.7.

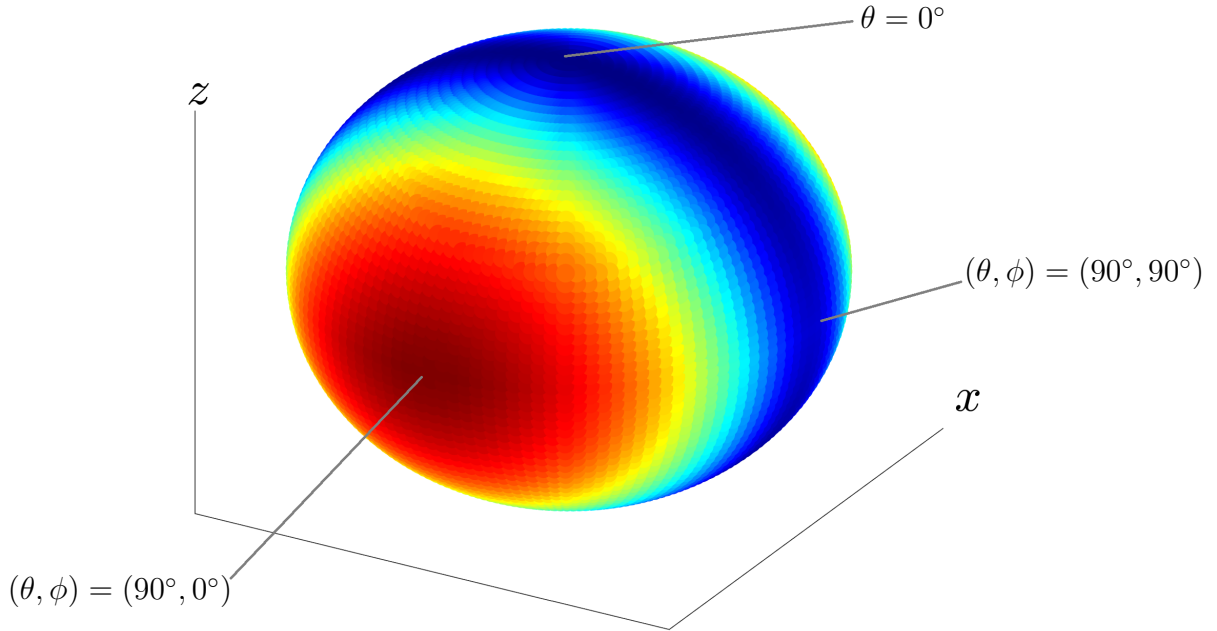


Figure 15: When G is small, the plasmonic response is basically dipolar and the electric field is strongest at the poles that are on the axis that has the same direction as the incident electric field.

9 Nonlinear Regime

We will now discuss the phenomenological range where the gain in the host medium is set above the linear amplification threshold. Since the dipole mode has been growing, the term $\Im(\mathbf{E}_{(2)} \cdot \Pi_{(2)}^*)$ will no longer be insignificant in the eq. 5.7: the system enters a non-linear growth regime. Since both $\mathbf{E}_{(2)}$ and $\Pi_{(2)}$ are spatially non-uniform fields (both are coordinate dependent), equation 5.7 indicates that the population inversion N will also adopt a non-uniform distribution and will no longer be approximately equal to \tilde{N} .

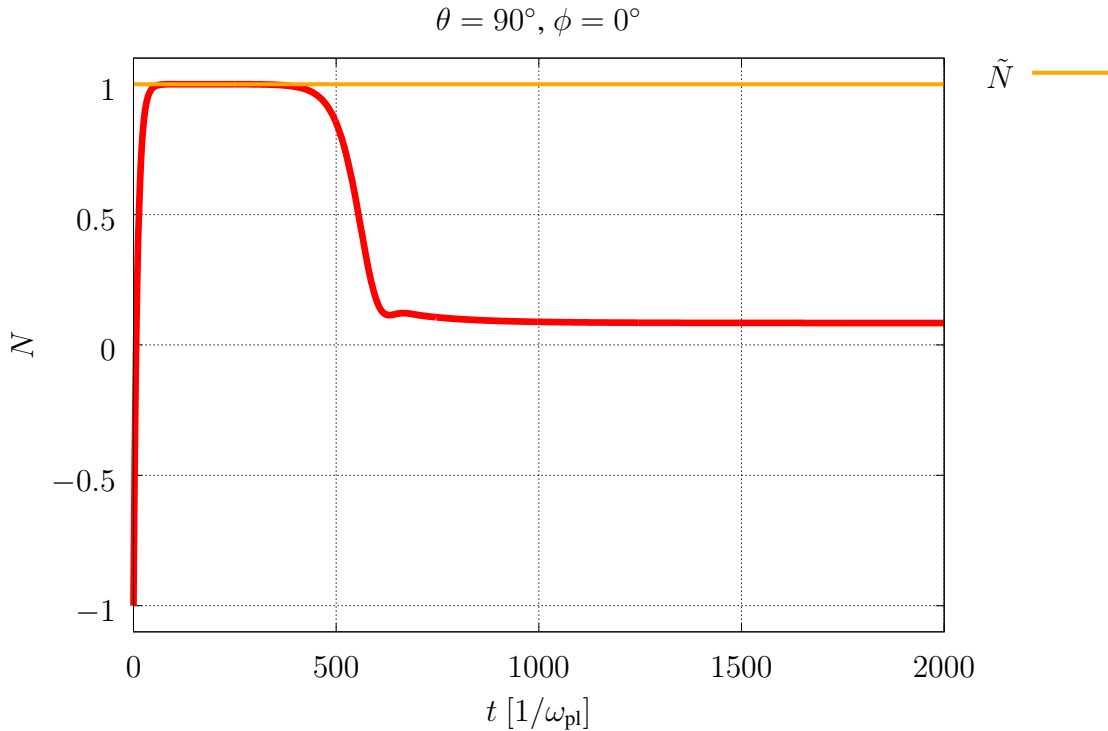


Figure 16: Temporal evolution of N for $G = -1$ and $\omega = \omega_{21}$. In the nonlinear regime, N no longer converges to a value approximately equal to \tilde{N} due to the competitive effect imposed by the term on the right hand side of equation 5.7 (which can be understood as a negative source term, no longer negligible as in the linear case, that causes the population inversion to be depleted).

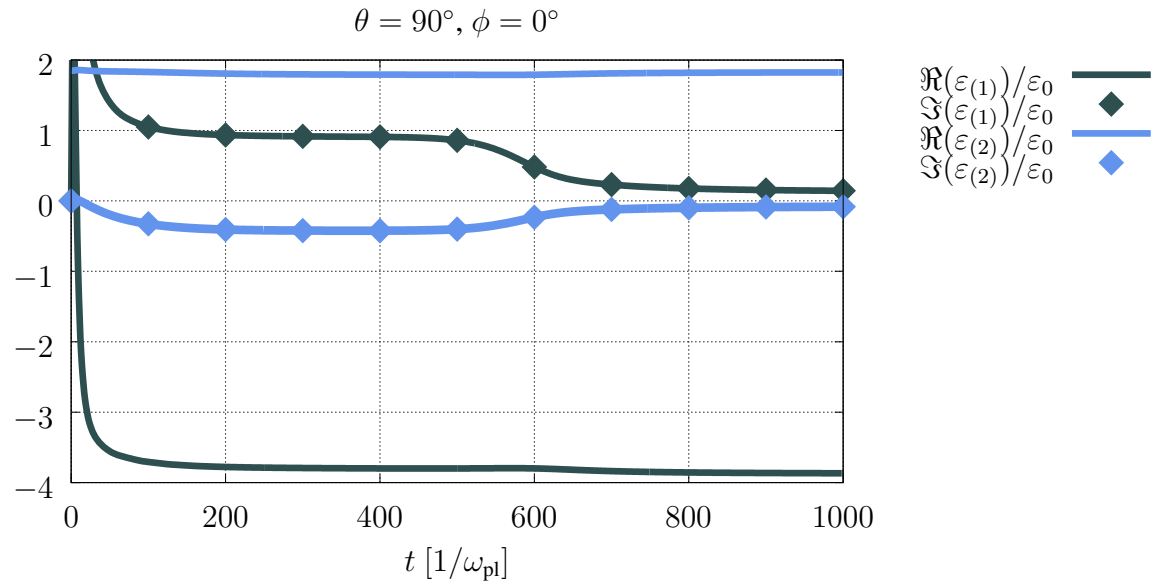


Figure 17: Evolution of the permittivities in the metal and the gain medium for $G = -1$ and $\omega = \omega_{21}$.

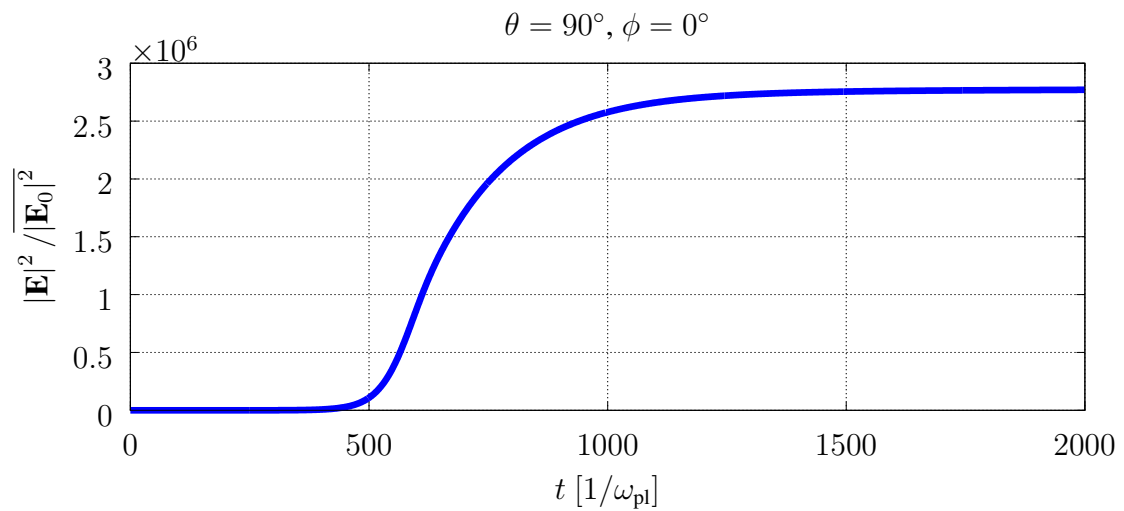


Figure 18: Time evolution of $|\mathbf{E}|^2 / |\mathbf{E}_0|^2$ when $G = -1$ and $\omega = \omega_{21}$.

$$\theta = 90^\circ, \phi = 0^\circ$$

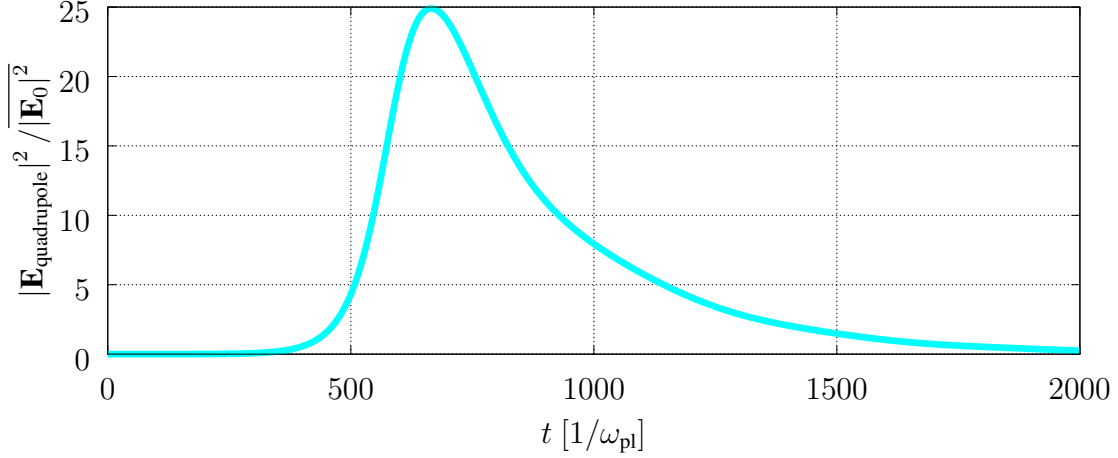


Figure 19: Time evolution of $|\mathbf{E}_{\text{quadrupole}}|^2 / |\overline{\mathbf{E}_0}|^2$ when $G = -1$ and $\omega = \omega_{21}$. In $|\mathbf{E}_{\text{quadrupole}}|^2$ only the terms with $J = 2$ are taken into account, which corresponds to the quadrupole term of the external field.

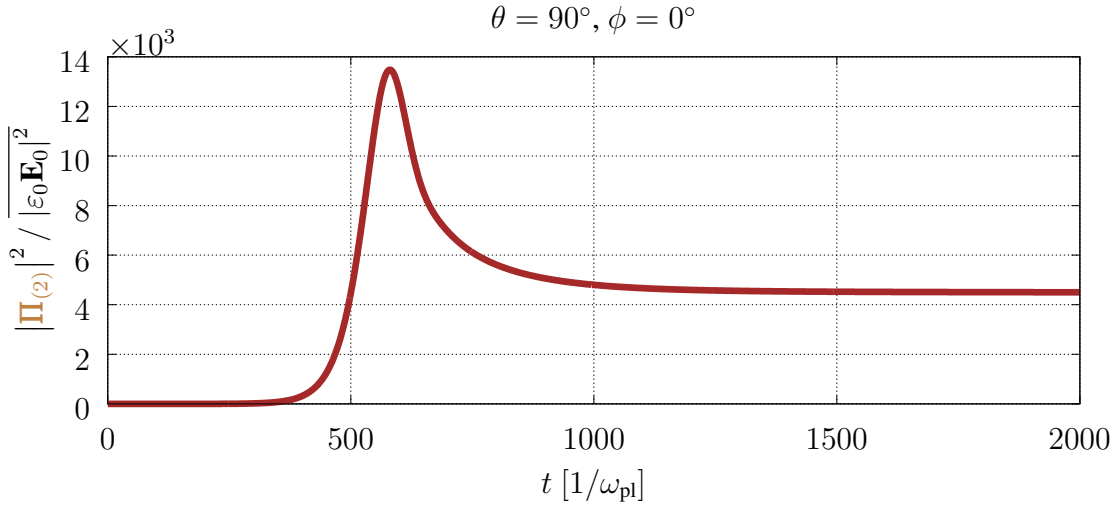


Figure 20: Time evolution of $|\Pi_{(2)}|^2 / |\varepsilon_0 \mathbf{E}_0|^2$ when $G = -1$ and $\omega = \omega_{21}$. $\mathbf{E} = \mathbf{E}_{(2)}$ and $\Pi_{(2)}$ are the electric field and the non-linear polarization term in the gain medium.

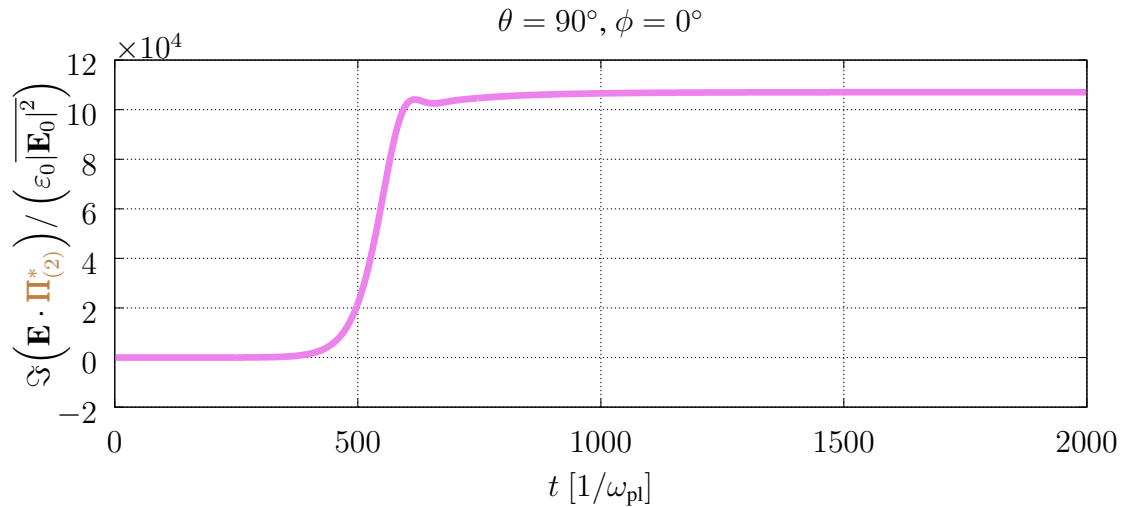


Figure 21: Time evolution of $\Im(\mathbf{E} \cdot \Pi_{(2)}^*) / (\varepsilon_0 |\mathbf{E}_0|^2)$ when $G = -1$ and $\omega = \omega_{21}$. $\mathbf{E} = \mathbf{E}_{(2)}$ and $\Pi_{(2)}$ are the electric field and the non-linear polarization term in the gain medium.

The oscillatory behavior of the fields (such as the oscillations in the external electric field shown in Fig. 22) corresponds to Rabi oscillations, which are typical of the dynamics that characterize the coherent interaction of a two-level system with light [13]. This dynamic is described by the Bloch equations and becomes evident in the nonlinear regime in which we fully use 5.6 and 5.7 without making approximations as in the linear case.

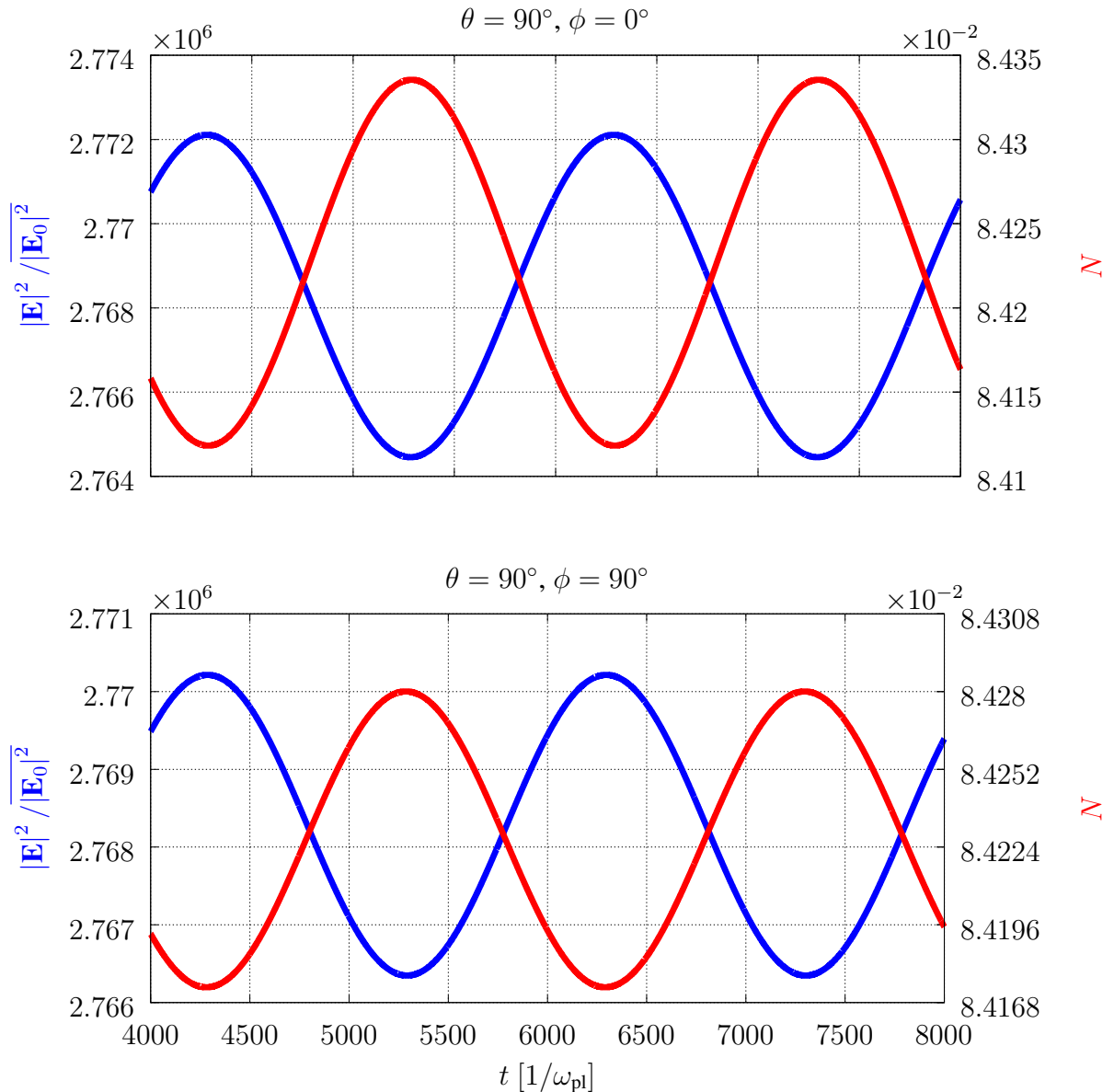


Figure 22: A close inspection of the temporal evolution of $|\mathbf{E}|^2$ and N shows that these quantities eventually oscillate with constant period. Also, when $|\mathbf{E}|^2$ has a maximum, N has a minimum.

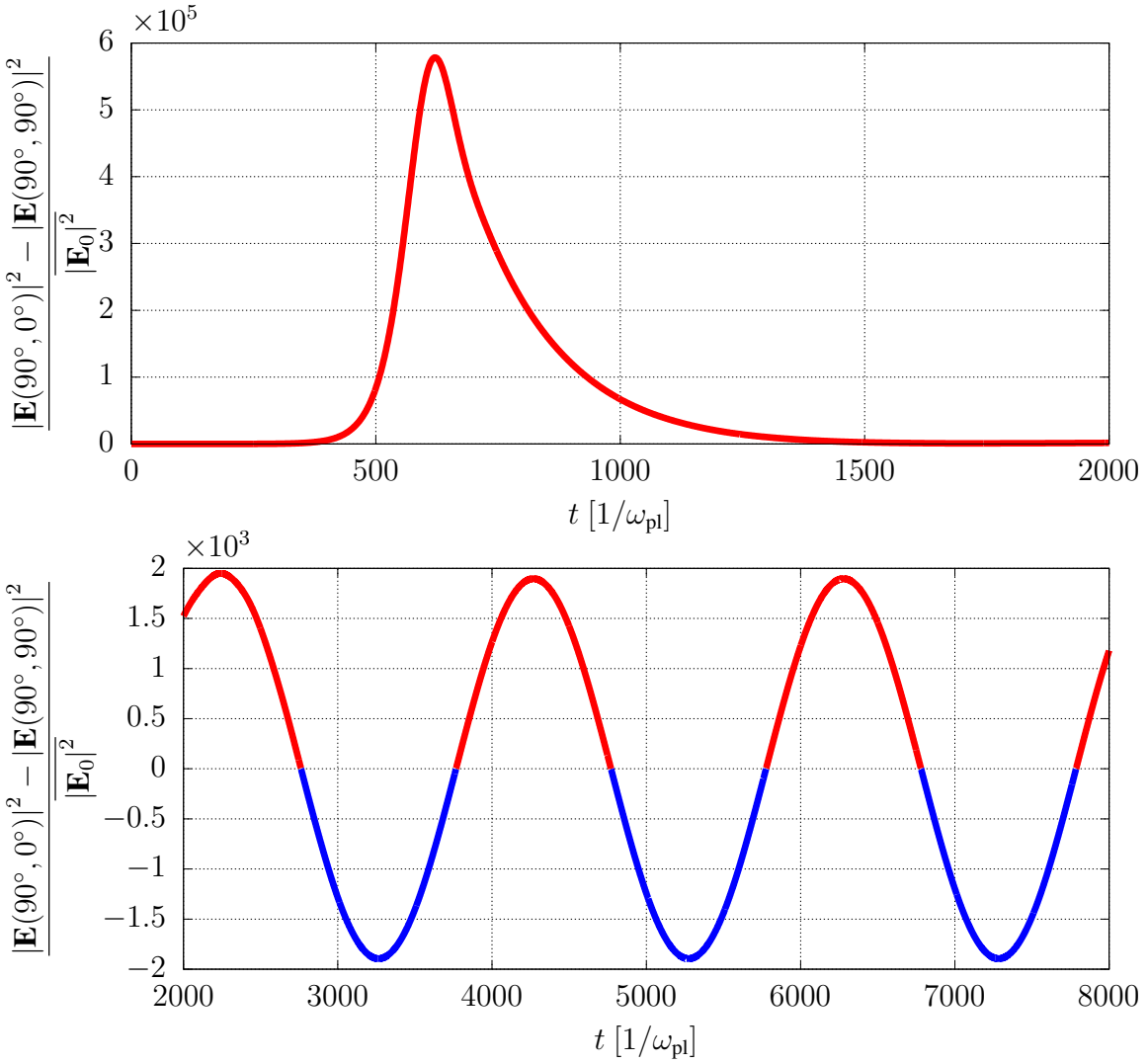


Figure 23: Difference between $|\mathbf{E}(\theta = 90^\circ, \phi = 0^\circ)|^2$ and $|\mathbf{E}(90^\circ, 90^\circ)|^2$. In the linear case, the energy was mostly concentrated at the poles of the sphere along the x -axis (the direction of the incident electric field). However, in this plot we note that, in certain periods of time, the field loses intensity along the x -axis to concentrate at other points on the surface of the nanosphere: at points on the plot where the difference is negative (blue), the electric field is more intense at the poles along the y -axis with respect to the poles along the x -axis. This is a sign of the emergence of other multipolar modes (see Fig. 28 to notice the momentary disappearance of the dipole character of the plasmonic response).

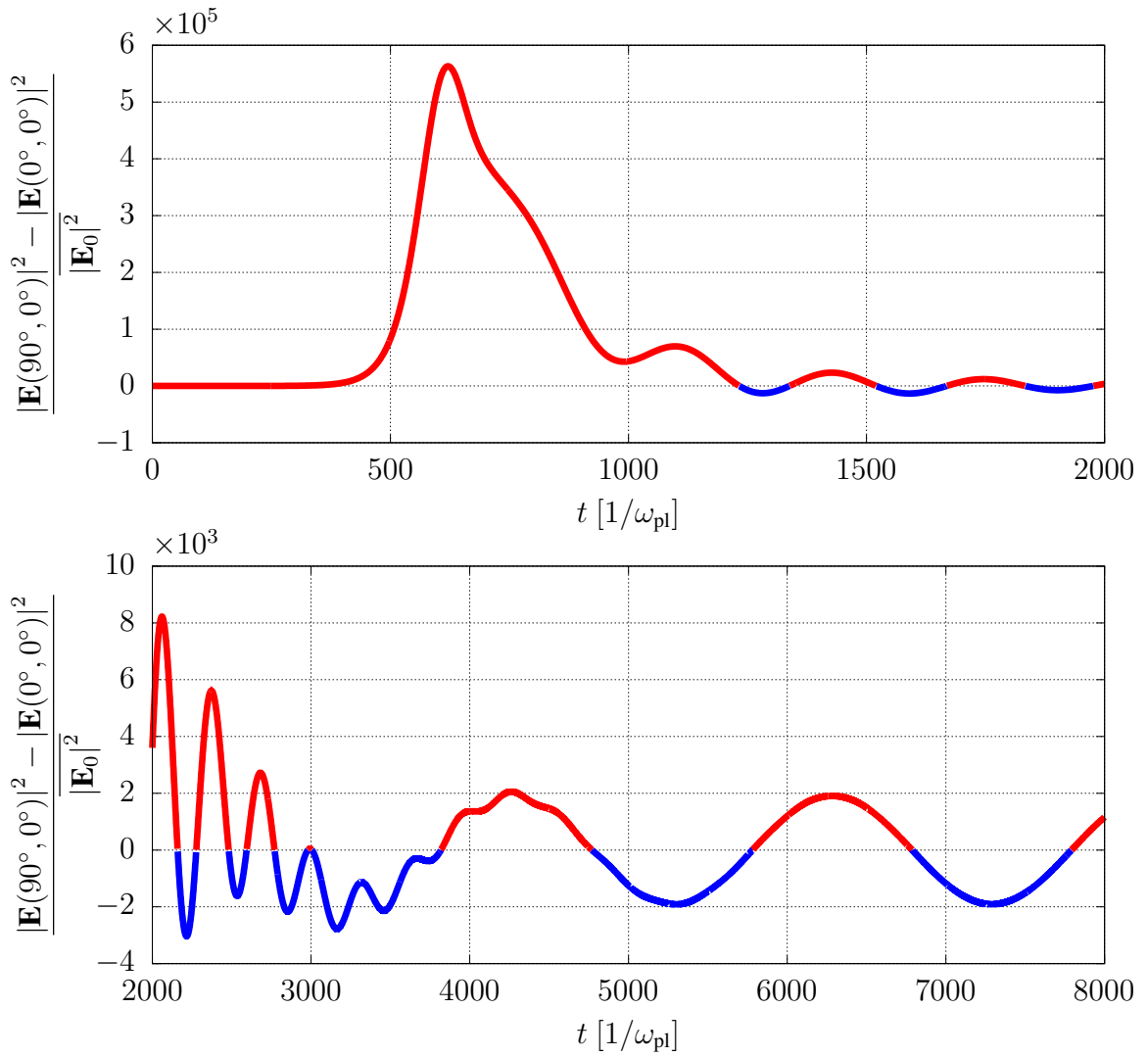


Figure 24: Difference between $|\mathbf{E}(90^\circ, 0^\circ)|^2$ and $|\mathbf{E}(0^\circ, 0^\circ)|^2$. At points on the plot where the difference is negative (blue), the electric field is more intense at the poles along the z -axis with respect to the poles along the x -axis.

$$\theta = 90^\circ, \phi = 0^\circ$$

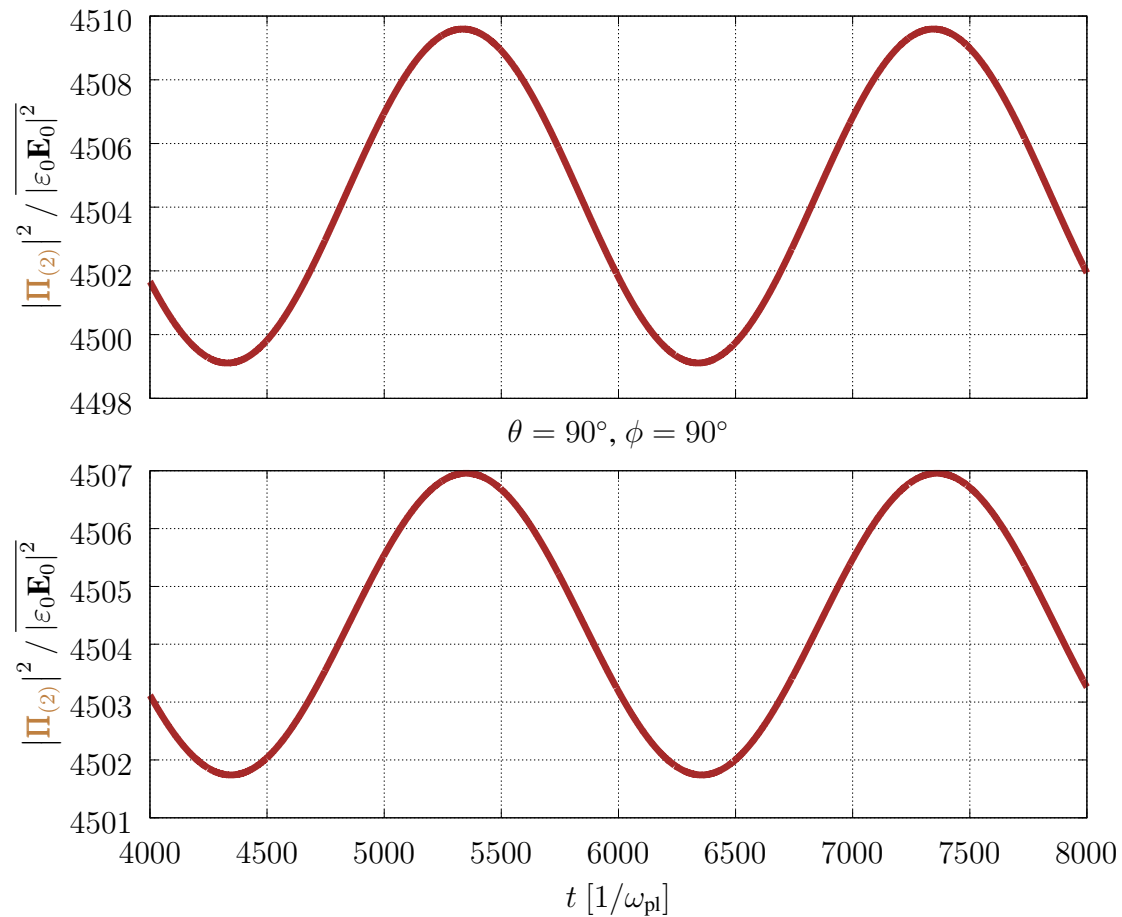


Figure 25: A close inspection of the temporal evolution of $|\Pi_{(2)}|^2$ shows that it oscillates.

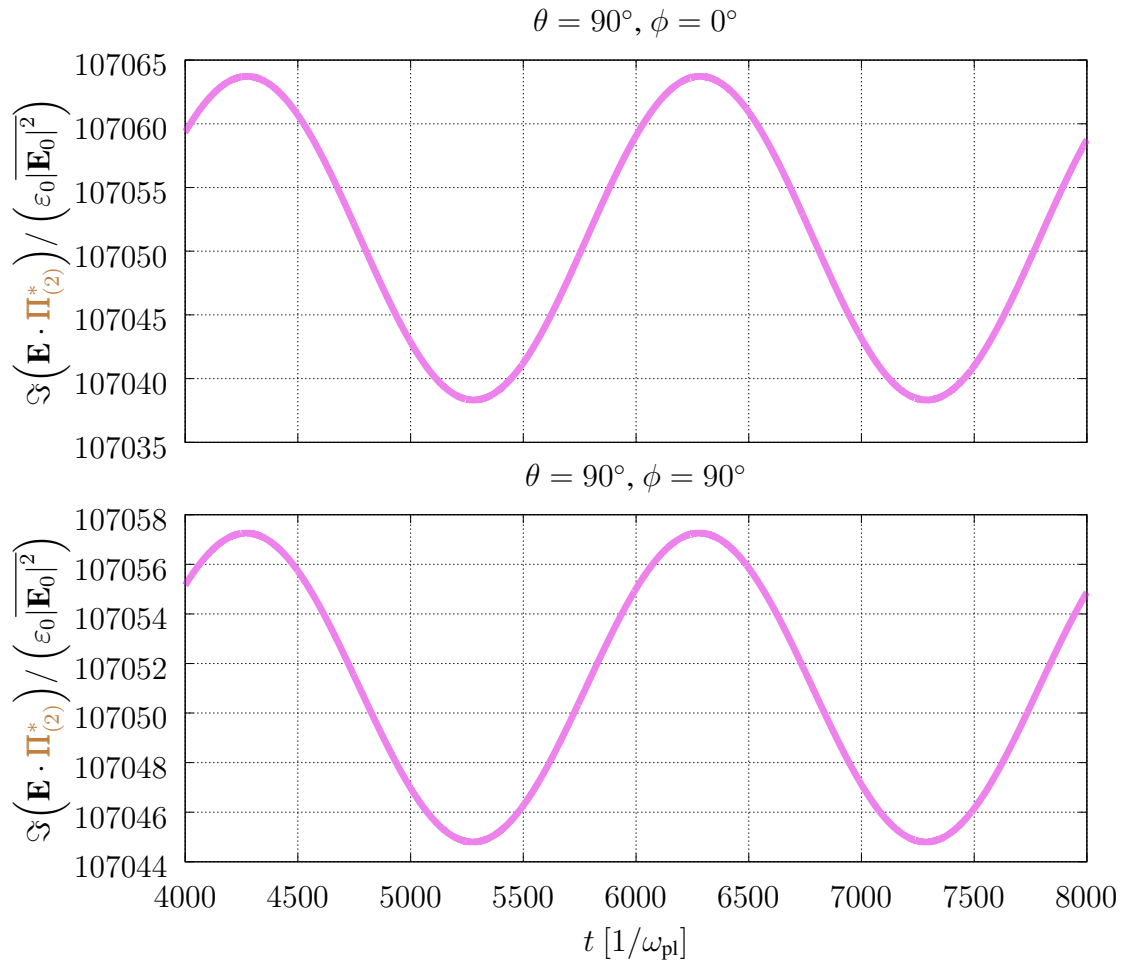


Figure 26: A close inspection of the temporal evolution of $\Im(\mathbf{E} \cdot \Pi_{(2)}^*)$ shows that it oscillates.

This term in Bloch's equation is initially insignificant and N is quickly driven to \tilde{N} because population inversion is continually restored; the pump can repopulate the upper level continuously. However, this term gets larger eventually, which means that the population inversion of the gain elements is depleted due to the energy absorbed by the plasmonic field.

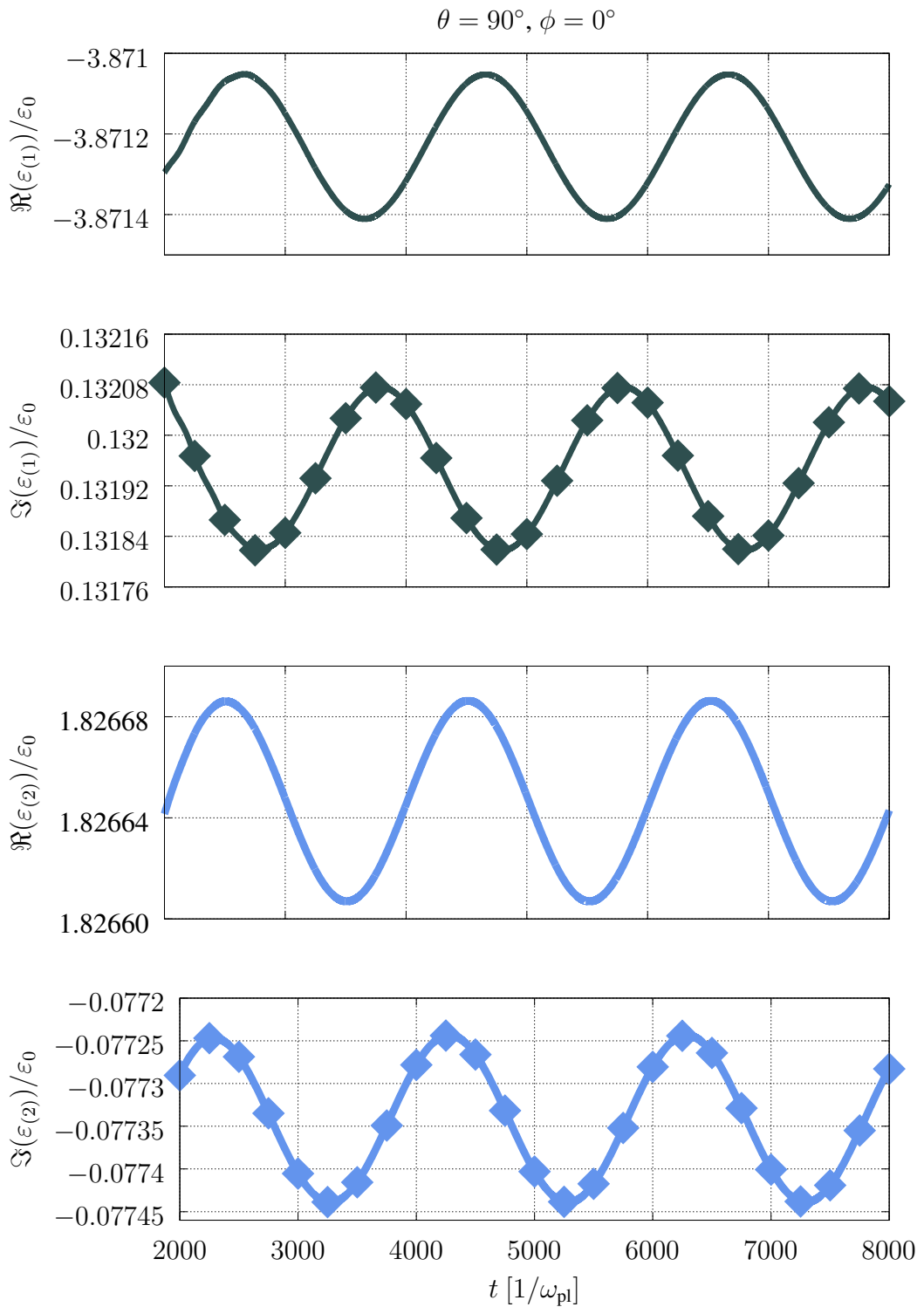


Figure 27: A closer inspection of the temporal evolution of the permitivities in the gain medium and in the metallic sphere.

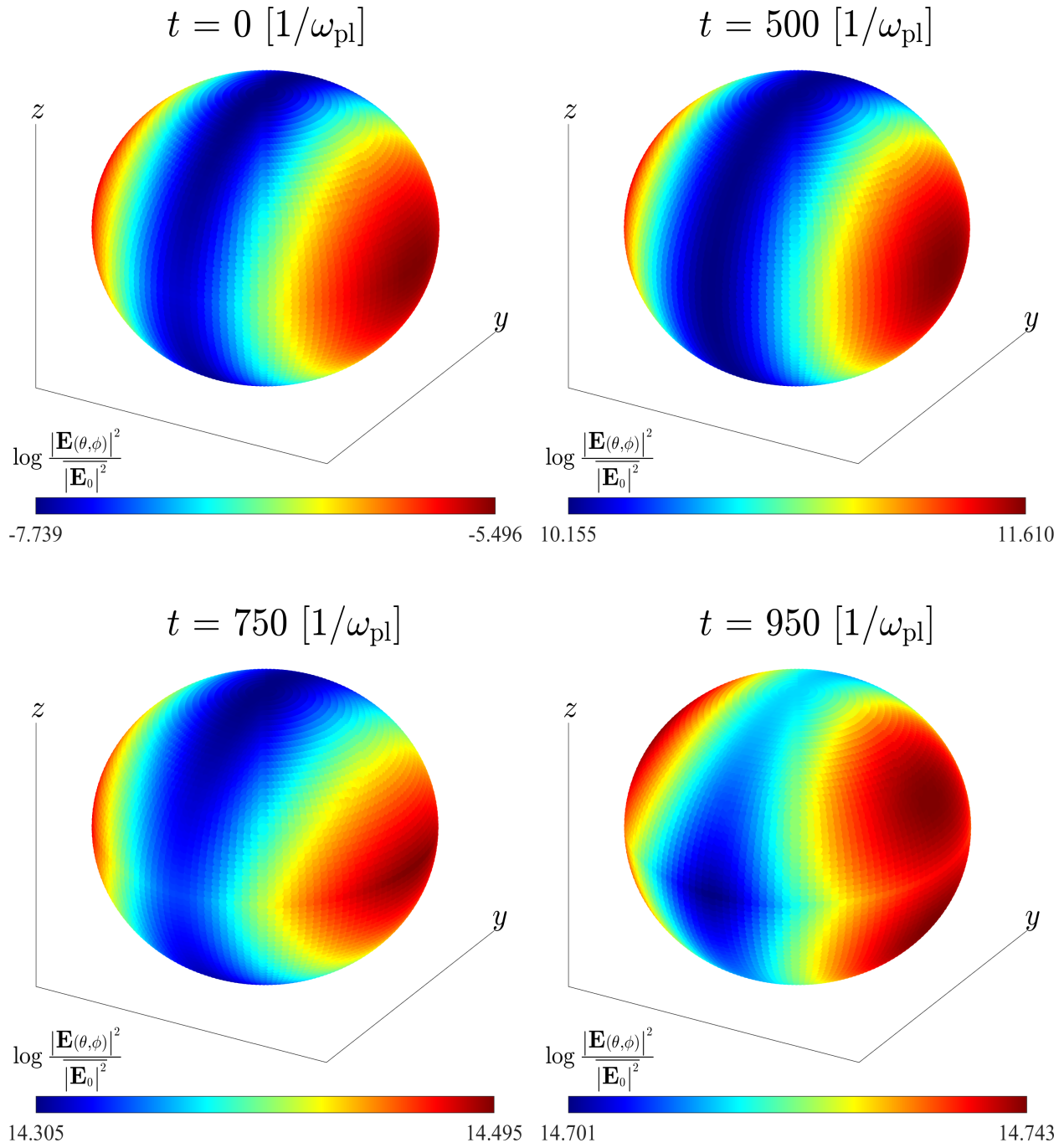
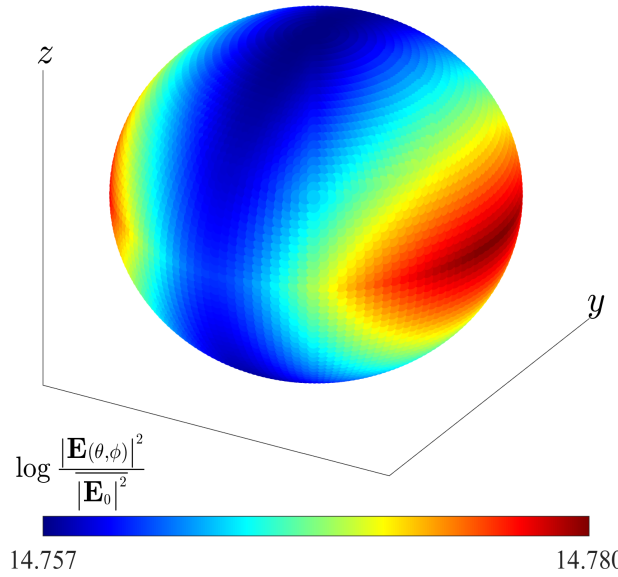
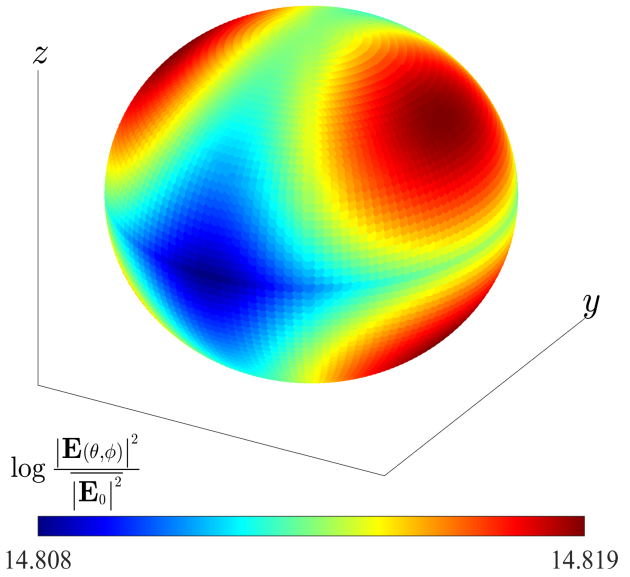


Figure 28: The plasmonic response is initially dipole, as is the case for small values of G . However, as the saturation process takes place, the dipolar mode is dissipated in parassite modes.

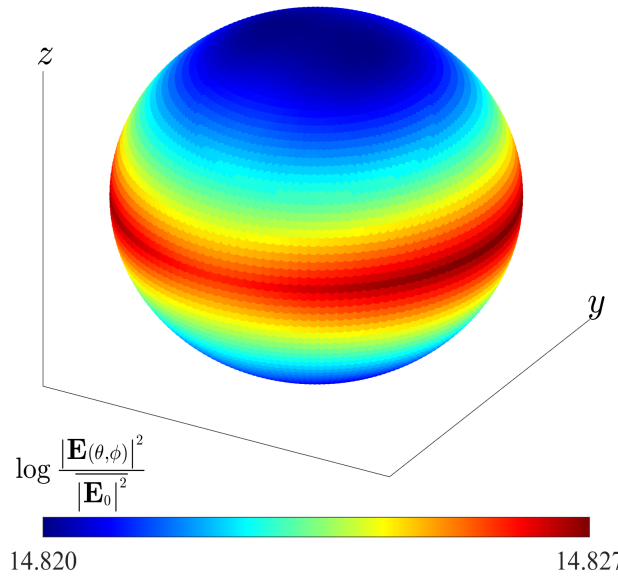
$t = 1050 [1/\omega_{\text{pl}}]$



$t = 1230 [1/\omega_{\text{pl}}]$



$t = 1450 [1/\omega_{\text{pl}}]$



$t = 1600 [1/\omega_{\text{pl}}]$

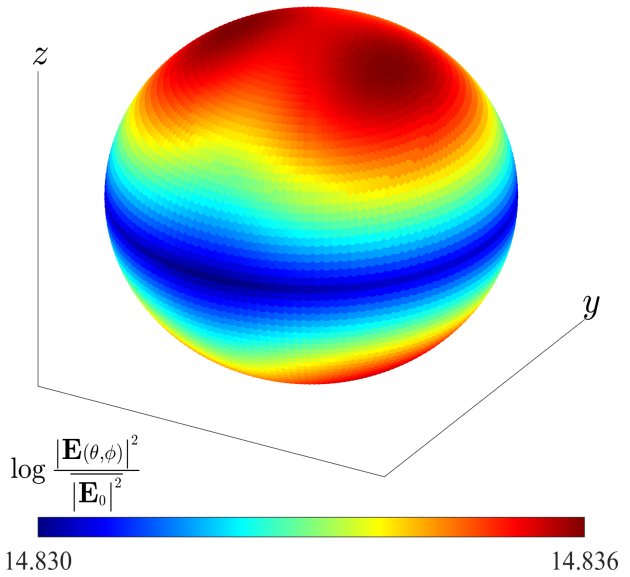
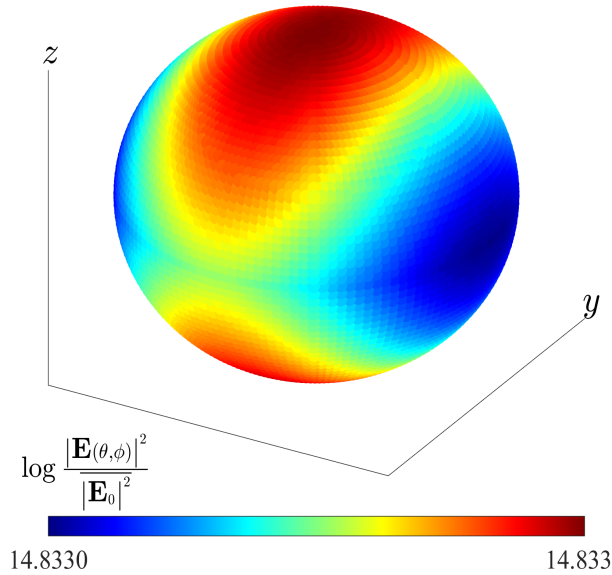
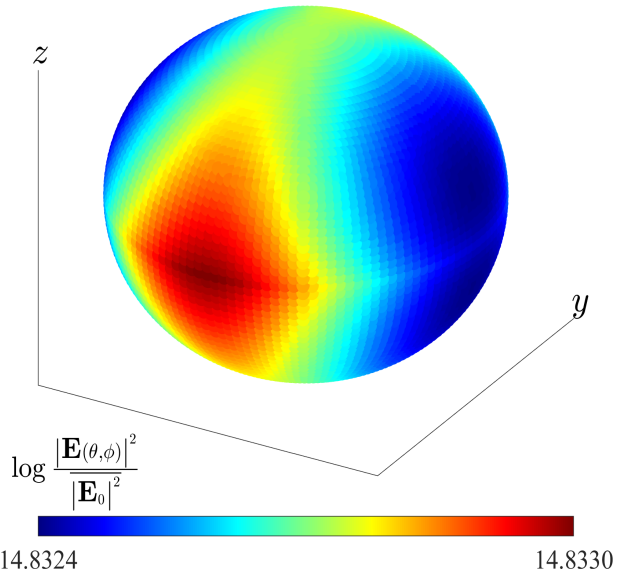


Figure 29: Continuation of Fig. 28.

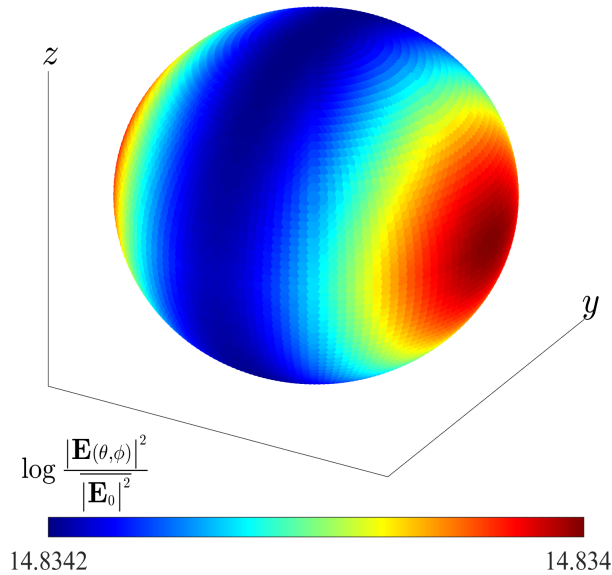
$t = 2900 [1/\omega_{\text{pl}}]$



$t = 3050 [1/\omega_{\text{pl}}]$



$t = 4300 [1/\omega_{\text{pl}}]$



$t = 5000 [1/\omega_{\text{pl}}]$

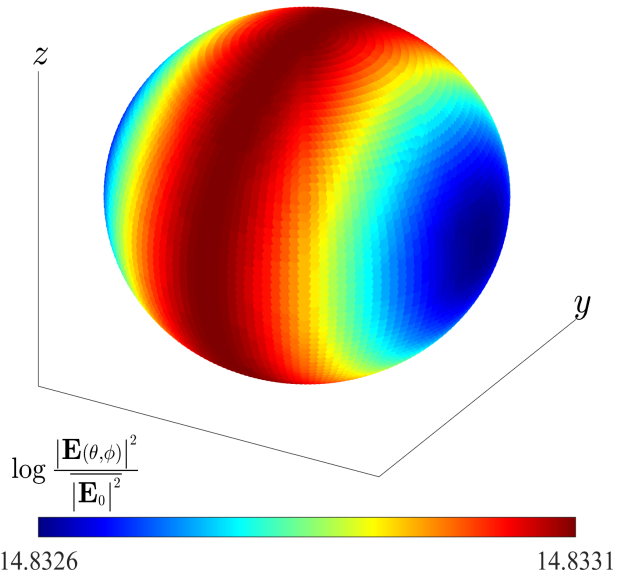


Figure 30: Continuation of Fig. 29.

10 Conclusions

In conclusion, a multipolar and dynamic model has been developed to quantitatively describe the optical response of a metallic nanosphere embedded in a gain medium. For low values of gain, the response of the system is a steady state. This is a linear amplification regime, where losses are partially compensated, allowing the plasmonic response to be amplified. This result is in correspondence with calculations obtained using a classical quasi-static formulation. However, when the gain values exceed a threshold, we have found that the population inversion of the gain elements is depleted due to the energy absorbed by the plasmonic field and that the dipole character of the nanoparticle response is lost, leading to a cascade of non-linear couplings that activates higher-order multipolar modes.

11 Future Work

Certainly the geometry of the nanoparticle has a non-negligible effect on the plasmonic response of the system. Therefore, it is recommended to adjust the model to describe more complicated geometries that are intended to be implemented in real designs. Depending on the type of application of interest, a multitude of geometries can be explored and optimized as a means of controlling the laser modes of the nano-emitter. Our analysis provides a way to determine how much gain will cause the system to go into a non-linear amplification regime, allowing in principle to design optical measurements geared to specific amplification rates in given geometries.

References

- [1] Hu, R., Yong, K.-T., Roy, I., Ding, H., He, S., & Prasad, P. N. (2009). Metallic Nanostructures as Localized Plasmon Resonance Enhanced Scattering Probes for Multiplex Dark-Field Targeted Imaging of Cancer Cells. *The Journal of Physical Chemistry C*, 113(7), 2676–2684.
- [2] Schuller, J. A., Barnard, E. S., Cai, W., Jun, Y. C., White, J. S., & Brongersma, M. L. (2010). Plasmonics for extreme light concentration and manipulation. *Nature Materials*, 9(3), 193–204.
- [3] Berini, P., & De Leon, I. (2011). Surface plasmon–polariton amplifiers and lasers. *Nature Photonics*, 6(1), 16–24.
- [4] Oulton, R. F., Sorger, V. J., Zentgraf, T., Ma, R.-M., Gladden, C., Dai, L., … Zhang, X. (2009). Plasmon lasers at deep subwavelength scale. *Nature*, 461(7264), 629–632.
- [5] Noginov, M. A., Zhu, G., Belgrave, A. M., Bakker, R., Shalaev, V. M., Narimanov, E. E., … Wiesner, U. (2009). Demonstration of a spaser-based nanolaser. *Nature*, 460(7259), 1110–1112.
- [6] Stockman, M. I. (2008). Spasers explained. *Nature Photonics*, 2(6), 327–329.
- [7] Strangi, G., De Luca, A., Ravaine, S., Ferrie, M., & Bartolino, R. (2011). Gain induced optical transparency in metamaterials. *Applied Physics Letters*, 98(25), 251912.
- [8] Veltri, A., Chipouline, A., & Aradian, A. (2016). Multipolar, time-dynamical model for the loss compensation and lasing of a spherical plasmonic nanoparticle spaser immersed in an active gain medium. *Scientific Reports*, 6(1).

- [9] D. A. Varshalovich, A. N. Moskalev, & V. K. Khersonskii. (2018). Quantum Theory of Angular Momentum. World Scientific, Singapore.
- [10] J. D. Jackson, Classical Electrodynamics, 3rd ed. (Wiley, New York, 1999).
- [11] Chipouline, A., Sugavanam, S., Fedotov, V. A., & Nikolaenko, A. E. (2012). Analytical model for active metamaterials with quantum ingredients. *Journal of Optics*, 14(11), 114005.
- [12] Maier, S. A. (2007). Plasmonics: Fundamentals and Applications.
- [13] Brandi, H. S., Latgé, A., Barticevic, Z., & Oliveira, L. E. (2005). Rabi oscillations in two-level semiconductor systems. *Solid State Communications*, 135(6), 386–389.

12 Appendices

12.1 Code to obtain the temporal evolution of the fields

After compiling this script, it can be run with the command `./Mie theta phi ome`, where the angles θ and ϕ are specified in radians (the analysis is done for a point on the surface of the nanosphere specified by these coordinates) and `ome` is $\hbar\omega$ in eV.

```
1 #include <iostream>
2 #include <iomanip>
3 #include <fstream>
4 #include <stdlib.h>
5 #include <sys/types.h>
6 #include <algorithm>
7 #include <complex_bessel.h>
8 #include <ctime>
9 #include <string>
10 #include <stdlib.h>
11 #include <math.h>
12 #include <boost/math/special_functions/spherical_harmonic.hpp>
13
14 // Compilation: g++ -Wall -I/usr/local/include -I/usr/include -L/
15 //               /usr/local/lib Mie.cxx -o Mie -lgsl -lgslcblas -lm -
16 //               lcomplex_bessel
17
18
19 double c=299792458;
```

```

20 double euler=2.718281828459045235360;
21 double h=6.626068e-34;
22 double j2eV=6.24150636309e18;
23 double eV2j=1.60217733000103e-19;
24
25 // Constants.
26 double PI = acos(-1);
27 double eps_0=8.8541878176e-12, gam, T1, T2, eps_inf=5.3*eps_0,
       n_density=1.e16, ome, ome_21, ome_pl; // Ag.
28 complex<double> img=complex<double> (0,1.);
29
30 // Variables.
31 complex<double> m, x, eps1_exact, eps2_exact, eps1, eps2, n1, n2,
       Nf=1., N=-1., f, g, alpha1, alpha2, polarizability, rabi;
32 double G=0; // Gain.
33 double ome_eV, omemi, omema, eps2_0, dome, time_M, freqG, sp_r,
       sp_ome_0, sp_dome; // NP.
34 double time_step=1.e0, time_current=0;
35 int J=1, M=1; // Indexes.
36 complex<double> B_in, C_in, D_in, B_sc, C_out, D_out, CC; //
   Coefficients.
37
38 // Angles.
39 double theta=0.523599, phi=0;
40
41 // Parameters.
42 long int N1=100, N2;
43 const int number_j = 5;
44 int it_max=8000, ome_an=50;
45 complex<double> coef[6][2*number_j]={};

```

```

46
47 // Files.
48 string name_file3_ome="GRAPH/N_t.dat";
49 ofstream file3 (name_file3_ome);           // N vs time.
50 string name_file4_ome="GRAPH/E2_2D.dat";
51 ofstream file4 (name_file4_ome, ofstream::app); // theta phi | E_ext|^2
52 string name_file5_ome="GRAPH/E2.dat";
53 ofstream file5 (name_file5_ome, ofstream::app); // x y z |E_ext|^2
54 string name_file6_ome="GRAPH/E2_t.dat";
55 ofstream file6 (name_file6_ome);           // |E_ext|^2 vs time
56 string name_file7_ome="GRAPH/alph_ome.dat";
57 ofstream file7 (name_file7_ome, ofstream::app); // alpha vs omega
58
59 // Bessel Functions.
60 complex<double> j (double order, complex<double> x)
61 {return sph_besselJ(order,x);}
62 complex<double> h1 (double order, complex<double> x)
63 {return sph_hankelH1(order, x);}
64
65 // Spherical Harmonics.
66 complex<double> Y (int J, int M, double theta, double phi)
67 {return boost::math::spherical_harmonic(J,M,theta,phi);}
68
69 // Components of the vector spherical harmonics.
70 complex<double> Yt1(int J, int M, double theta, double phi)
71 {return 0.5*sqrt((J-M)*(J+M+1)/(J*(J+1)))*pow(euler,-img*phi)*Y(J
    ,M+1,theta,phi)-0.5*sqrt((J+M)*(J-M+1)/(J*(J+1)))*pow(euler,
    img*phi)*Y(J,M-1,theta,phi);}

```

```

72
73 complex<double> Yp1(int J, int M, double theta, double phi)
74 {return img*(double)M*Y(J,M,theta,phi)/(sqrt(J*(J+1))*sin(theta))
75 ;
76 complex<double> Yt0(int J, int M, double theta, double phi)
77 {return -(double)M*Y(J,M,theta,phi)/(sqrt(J*(J+1))*sin(theta));}
78
79 complex<double> Yp0(int J, int M, double theta, double phi)
80 {return -img*0.5*sqrt((J-M)*(J+M+1)/(J*(J+1)))*pow(euler,-img*phi
81 )*Y(J,M+1,theta,phi)+img*0.5*sqrt((J+M)*(J-M+1)/(J*(J+1)))*pow
82 (euler,img*phi)*Y(J,M-1,theta,phi);}
83 // Dot product.
84 complex<double> Y1_Y1(int J1, int M1, int J2, int M2, double
85 theta, double phi)
86 {return Yt1(J1,M1,theta,phi)*conj(Yt1(J2,M2,theta,phi))+Yp1(J1,
87 M1,theta,phi)*conj(Yp1(J2,M2,theta,phi));}
88 complex<double> Y1_Y0(int J1, int M1, int J2, int M2, double
89 theta, double phi)
90 {return Yt1(J1,M1,theta,phi)*conj(Yt0(J2,M2,theta,phi))+Yp1(J1,
91 M1,theta,phi)*conj(Yp0(J2,M2,theta,phi));}
92 complex<double> Y0_Y1(int J1, int M1, int J2, int M2, double
93 theta, double phi)
94 {return Yt0(J1,M1,theta,phi)*conj(Yt1(J2,M2,theta,phi))+Yp0(J1,
95 M1,theta,phi)*conj(Yp1(J2,M2,theta,phi));}
96 complex<double> Y0_Y0(int J1, int M1, int J2, int M2, double
97 theta, double phi)
98 {return Yt0(J1,M1,theta,phi)*conj(Yt0(J2,M2,theta,phi))+Yp0(J1,
99 M1,theta,phi)*conj(Yp0(J2,M2,theta,phi));}

```

```

91 complex<double> Yn_Yn(int J1, int M1, int J2, int M2, double
    theta, double phi)
92 {return Y(J1,M1,theta,phi)*conj(Y(J2,M2,theta,phi));}
93
94 // Riccati-Bessel Functions.
95 complex<double> RBj (double order, complex<double> x)
96 {return x*sph_besselJ(order,x);}
97 complex<double> RBj_prime (double order, complex<double> x)
98 {return (x*sph_besselJ(order-1,x)-order*sph_besselJ(order,x));}
99
100 complex<double> RBh (double order, complex<double> x)
101 {return x*sph_hankelH1(order, x);}
102 complex<double> RBh_prime (double order, complex<double> x)
103 {return (x*sph_hankelH1(order-1,x)-order*sph_hankelH1(order,x));}
104
105 // Coupled RK4: To solve coupled equations of the form      df1/dt
106 //                  +a1*f1+b1*f2+c1=0,      df2/dt+a2*f1+b2*f2+c2=0.
107 complex<double> RK4_coupled (complex<double> f1, complex<double>
    f2, complex<double> a1, complex<double> b1, complex<double> c1
    , complex<double> a2, complex<double> b2, complex<double> c2,
    int index)
108     {complex<double> k11=time_step*(-a1*f1-b1*f2-c1), k12=
        time_step*(-a2*f1-b2*f2-c2);
109     complex<double> k21=time_step*(-a1*(f1+0.5*k11)-b1*(f2+0.5*
        k12)-c1), k22=time_step*(-a2*(f1+0.5*k11)-b2*(f2+0.5*k12)-
        c2);
110     complex<double> k31=time_step*(-a1*(f1+0.5*k21)-b1*(f2+0.5*
        k22)-c1), k32=time_step*(-a2*(f1+0.5*k21)-b2*(f2+0.5*k22)-
        c2);
111     complex<double> k41=time_step*(-a1*(f1+k31)-b1*(f2+k32)-c1),

```

```

        k42=time_step*(-a2*(f1+k31)-b2*(f2+k32)-c2);

111    f1=f1+(1/6.)*(k11+2.*k21+2.*k31+k41); f2=f2+(1/6.)*(k12+2.*
        k22+2.*k32+k42);

112    if(index==0){return f1;} else if(index==1){return f2;} else{
        return 0; }

113

114 // RK4: To solve equations of the form      df1/dt+a1*f1+b1=0.

115 complex<double> RK4 (complex<double> f1, complex<double> a1,
        complex<double> b1)
116    {complex<double> k1=time_step*(-a1*f1-b1);
117     complex<double> k2=time_step*(-a1*(f1+0.5*k1)-b1);
118     complex<double> k3=time_step*(-a1*(f1+0.5*k2)-b1);
119     complex<double> k4=time_step*(-a1*(f1+k3)-b1);
120     f1=f1+(1/6.)*(k1+2.*k2+2.*k3+k4);
121     return f1; }

122

123 // Incident "inc" wave coefficients.

124 complex<double> a_inc (int J, int M)
125     {if(M==1 || M==-1){return 1;}
126     else {return 0;}}
127 complex<double> b_inc (int J, int M)
128     {if(M==1){return -img; }
129     else if (M==-1){return img; }
130     else {return 0;}}
131

132 // Internal "in" wave coefficients.

133 complex<double> a_in (int J, int M)
134     {return a_inc(J,M)*(j(J,x)*RBh_prime(J,x)-h1(J,x)*RBj_prime(J
        ,x))/ (j(J,m*x)*RBh_prime(J,x)-h1(J,x)*RBj_prime(J,m*x));}
135 complex<double> b_in (int J, int M)

```

```

136 {complex<double> coef4 = img*eps_0*N / ( 2*T2*Nf*h1(J,x)*(-
137     img*(ome-ome_21)+1./T2) );
138 coef4 = eps2_0*eps_0 + 2.*h1(J,x)*coef4;
139 return m*b_inc(J,M)*( coef4*(j(J,x)*RBh_prime(J,x)-h1(J,x)*
140     RBj_prime(J,x)) / ( (eps_inf-eps_0*pow(ome_pl,2)/(pow(
141     ome,2)+2.*img*gam*ome))*j(J,m*x)*RBh_prime(J,x)-coef4*h1(J
142 ,x)*RBj_prime(J,m*x) ); }
143 complex<double> c_in (int J, int M)
144 {return -a_in(J,M)*eps_0*pow(ome_pl,2)/(pow(ome,2)+2.*img*gam
145 *ome); }
146 complex<double> d_in (int J, int M)
147 {return -b_in(J,M)*eps_0*pow(ome_pl,2)/(pow(ome,2)+2.*img*gam
148 *ome); }
149
150
151 // Scattered "sc" wave coefficients
152 complex<double> a_sc (int J, int M)
153 {return a_inc(J,M)*(j(J,m*x)*RBj_prime(J,x)-j(J,x)*RBj_prime(
154     J,m*x))/ (h1(J,x)*RBj_prime(J,m*x)-j(J,m*x)*RBh_prime(J,x))
155 ; }
156 complex<double> b_sc (int J, int M)
157 {return (b_in(J,M)*RBj_prime(J,m*x)/m-b_inc(J,M)*RBj_prime(J,
158     x))/RBh_prime(J,x); }
159
160
161 // External "out" wave coefficients
162 complex<double> c_out (int J, int M)
163 {return img*eps_0*N*(j(J,x)*a_inc(J,M)+h1(J,x)*a_sc(J,M) )
164     /(2.*T2*Nf*h1(J,x)*(-img*(ome-ome_21)+1./T2)); }
165 complex<double> d_out (int J, int M)
166 {return img*eps_0*N*(j(J,x)*b_inc(J,M)+h1(J,x)*b_sc(J,M) )

```

```

    / (2.*T2*Nf*h1(J,x)*(-img*(ome-ome_21)+1./T2)); }

156
157
158 complex<double> * Mie(int J, int M, int i, int it)
159 {
160     static complex<double> for_product[6]={}; // b_sc c_out d_out
161     b_in c_in d_in
162     // Analysis.
163     if(it%100==0){cout<<"\n***Coefficients for J = "<<J<<" and M
164         = "<<M<<endl;}
165
166
167     T2=h/(PI*eV2*j*sp_dome);
168     T1=0.1*T2;
169
170
171     ome_21=sp_ome_0*2.*PI*eV2*j/h;
172     ome=2.*PI*eV2*j*ome_eV/h;      // Frequency in SI units.
173     gam=2.*PI*eV2*j*0.0228/h;      // Drude.
174
175
176     eps1_exact=eps_inf-eps_0*pow(ome_pl,2)/(pow(ome,2)+2.*img
177         *gam*ome);      // Metal.
178     eps2_exact=eps_0*(eps2_0-(N/Nf)*G*(2/T2)/(2*(ome-ome_21)-
179         img*(2/T2))); // External medium.
180
181     if(it==0){eps1=eps1_exact;eps2=eps2_exact;}
182
183
184     n1=sqrt(eps1/eps_0);           // Internal refractive
185         index.
186     n2=sqrt(eps2/eps_0);           // External refractive
187         index.
188     m=n1/n2;                      // Relative refractive index.

```

```

179         x=sp_r*ome*n2/c;           // k_ext*a.
180         alpha2=img/(ome*n2/c);    // i/k_ext.
181         alpha1=alpha2/m;          // i/k_int.
182         double lam=h*c/(ome_eV*eV2j); // Wavelength.
183
184         // Predicted values for the linear case.
185         complex<double> E_ain = a_in(J,M), E_bin = b_in(J,M),
186             E_cin = c_in(J,M), E_din = d_in(J,M), E_ainc = a_inc(J
187             ,M),
188         E_binc = b_inc(J,M), E_asc = a_sc(J,M), E_bsc = b_sc(J,M)
189             , E_cout = c_out(J,M), E_dout = d_out(J,M);
190
191         if(it%100==0) {
192             cout<<"PREDICTED"<<endl;
193             cout<<"Incident electric field E_inc: a = "<<E_ainc<<" b
194             = "<<E_binc<<endl;
195             cout<<"Internal electric field E_in: a = "<<E_ain<<" b =
196                 "<<E_bin<<" c = "<<E_cin<<" d = "<<E_din<<endl;
197             cout<<"Scattered electric field E_sc: a = "<<E_asc<<" b =
198                 "<<E_bsc<<endl;
199             cout<<"External polarizability P_out: c = "<<E_cout<<" d
200                 = "<<E_dout<<endl; }
201
202         // Normalization.
203         ome=ome/ome_pl; gam=gam/ome_pl; lam=lam/sp_r; ome_21=
204             ome_21/ome_pl; T1=T1*ome_pl; T2=T2*ome_pl; //
205             Normalization.
206
207         // Initial conditions.
208         if(M===-1) {B_in=coef[0][J-1]; C_in=coef[1][J-1]; D_in=coef

```

```

[2][J-1]; B_sc=coef[3][J-1]; C_out=coef[4][J-1]; D_out
=coef[5][J-1];}

200   if(M==1) {B_in=coef[0][J+number_j-1]; C_in=coef[1][J+
number_j-1]; D_in=coef[2][J+number_j-1]; B_sc=coef[3][
J+number_j-1]; C_out=coef[4][J+number_j-1]; D_out=coef
[5][J+number_j-1];}

201

202   if(it<=1){B_in=0; C_in=0; D_in=0; B_sc=0; C_out=0; D_out
=0; }

203

204 // Coefficients for coupled RK4.

205 complex<double> coef1 = eps2_0*eps_0*E_binc*(j(J,x)-
h1(J,x)*RBj_prime(J,x)/RBh_prime(J,x)),

206     coef2 = eps2_0*eps_0*h1(J,x)*RBj_prime(J,m*x)
/RBh_prime(J,x)-eps_inf*j(J,m*x),
207     coef3 = img*eps_0*G*N/(2.*T2*Nf),
208     a1 = -(pow(ome,2)+2.*img*gam*ome)/(2.*(gam-img
*ome))-eps_0*j(J,m*x)/(coef2*2.*(gam-img*ome))

209     ,
210     b1 = eps_0*m*h1(J,x)/(coef2*(gam-img*ome)),
211     c1 = eps_0*m*coef1/(coef2*2.*(gam-img*ome)),
212     a2 = -coef3*j(J,m*x)*RBj_prime(J,m*x)/(m*coef2
*RBh_prime(J,x)),
213     b2 = -img*(ome-ome_21)+1./T2+2.*coef3*pow(h1(J
,x),1)*RBj_prime(J,m*x)/(coef2*RBh_prime(J,x))
214     ,
215     c2 = (coef1*coef3)/(h1(J,x))*(h1(J,x)*
RBj_prime(J,m*x)/(coef2*RBh_prime(J,x))-1./(eps2_0*eps_0));

```

```

215 // Time evolution.
216 for(int z=0; z<=N2; z++) {
217     time_current=time_step*z; //Current iteration.
218
219     D_in      = RK4_coupled( D_in, D_out, a1, b1, c1, a2,
220                               b2, c2, 0 );
220     D_out     = RK4_coupled( D_in, D_out, a1, b1, c1, a2,
221                               b2, c2, 1 );
221
222     B_in      = (D_in*j(J,m*x)-2.*m*D_out*h1(J,x)-m*coef1
223                               )/coef2;
224
225     B_sc      = (B_in*RBj_prime(J,m*x)/m-E_binc*RBj_prime
226                               (J,x))/RBh_prime(J,x);
227
228
229     C_in      = RK4( C_in, -(pow(ome,2)+2.*img*gam*ome)
230                               /(2.*(gam-img*ome)), -eps_0*E_ain/(2.*(gam-img*ome
231                               )) );
232
233     C_out     = RK4( C_out, -img*(ome-ome_21)+1./T2, -(

234                               coef3/h1(J,x))*(j(J,x)*E_ainc+h1(J,x)*E_asc) );
235
236     }time_current=0; // END: Time evolution.
237
238
239     if(it==0){B_in=0; C_in=0; D_in=0; B_sc=0; C_out=0; D_out
240                               =0; }
241
242     for_product[0]=B_sc; for_product[1]=C_out; for_product
243                               [2]=D_out; for_product[3]=B_in; for_product[4]=C_in;
244     for_product[5]=D_in;
245
246     if(M===-1){coef[0][J-1]=B_in; coef[1][J-1]=C_in; coef[2][J
247                               -1]=D_in; coef[3][J-1]=B_sc; coef[4][J-1]=C_out; coef
248                               [5]=D_out; }

```

```

[5] [J-1]=D_out; }

234 if (M==1) {coef[0][J+number_j-1]=B_in; coef[1][J+number_j
-1]=C_in; coef[2][J+number_j-1]=D_in; coef[3][J+
number_j-1]=B_sc; coef[4][J+number_j-1]=C_out; coef
[5][J+number_j-1]=D_out; }

235

236 // Printing the results.

237 if(it%100==0){

238 cout<<"CALCULATED"<<endl;
239 cout<<"Incident electric field E_inc: a = "<<E_ainc<<" b
= "<<E_binc<<endl;
240 cout<<"Internal electric field E_in: a = "<<E_ain<<" b =
" <<B_in<<" c = "<<C_in<<" d = "<<D_in<<endl;
241 cout<<"Scattered electric field E_sc: a = "<<E_asc<<" b =
" <<B_sc<<endl;
242 cout<<"External polarizability P_out: c = "<<C_out<<" d =
" <<D_out<<endl; }

243

244 if(it==it_max&&J==1&&M==1){

245 file4<<theta*180./PI<<" "<<phi*180./PI<<" "<<norm(f)<<' \n
'; file4<<180.-theta*180./PI<<" "<<phi*180./PI<<" "<<
norm(f)<<' \n';
246 file4<<theta*180./PI<<" "<<360.-phi*180./PI<<" "<<norm(f)
<<' \n'; file4<<180.-theta*180./PI<<" "<<360.-phi*180./
PI<<" "<<norm(f)<<' \n';
247 file5<<sin(theta)*cos(phi)<<" "<<sin(theta)*sin(phi)<<" "
<<cos(theta)<<" "<<norm(f)<<' \n'; file5<<sin(theta)*
cos(phi)<<" "<<sin(theta)*sin(phi)<<" "<<-cos(theta)<<
" "<<norm(f)<<' \n';
248 file5<<-sin(theta)*cos(phi)<<" "<<-sin(theta)*sin(phi)<<" "

```

```

        " <<cos(theta) <<" " <<norm(f) <<' \n' ; file5 <<-sin(theta)
        *cos(phi) <<" " <<-sin(theta)*sin(phi) <<" " <<-cos(theta)
        <<" " <<norm(f) <<' \n' ; }

249
250     // END: Analysis.
251
252 } // END: Mie
253
254 int main (int argc, char* argv[])
255 {
256     // Angles.
257     theta=strtod(argv[1], NULL); phi=strtod(argv[2], NULL);
258     omega_eV=strtod(argv[3], NULL);
259
260     // Nanoparticle.
261     fstream nano;
262     nano.open ("in/nanosphere_eV.dat", ios::in);
263     nano>>sp_r>>sp_dome>>sp_omega_0>>G>>omega_mi>>omega_ma;
264
265     N2=int (time_M);
266     sp_r*=1.e-9;           // Radius of the sphere in m.
267     eps2_0=1.8496;         // Ethanol.
268     dome=(omega_ma-omega_mi)/N1;
269     omega_pl=2.*PI*eV2j*9.6/h;    // Plasma frequency.
270
271     if (G<0.) { n_density*=abs(G); }
272
273     complex<double> PRODUCT_EP = 0, PRODUCT_EE = 0, PRODUCT_EP_in
274     = 0, PRODUCT_EE_in = 0;
275     complex<double> for_product[12][number_j]={};

```

```

274
275 // Introduction.
276 cout<<"\nAnalysis for G = "<<G<<" theta = "<<theta*180./PI<<
277           phi = "<<phi*180./PI<<" ome = "<<ome_eV<<" \n"<<endl;
278
279 clock_t begin = clock(); // Time measurement starts.
280
281 // Analysis.
282 for(int it = 0; it<=it_max; it++) {
283   cout<<"\nIT: "<<it<<endl;
284   cout<<"Current N: "<<N<<endl;
285
286   file3<<it*time_step<< " "; file3<<scientific<<setprecision(10)
287   <<real(N)<< " "<<real(Nf)<<"\n";
288
289   for(int jj = 1; jj<=number_j; jj++) {
290     for(int mm = -1; mm<=1; mm=mm+2) {
291       //cout<<"***Numbers J M: "<<jj<<" "<<mm<<endl;
292       complex<double> *result_mie;
293       result_mie=Mie(jj,mm,ome_an,it);
294       if(mm==1) {for_product[0][jj-1]=*(result_mie); for_product[1][
295         jj-1]=*(result_mie+1); for_product[2][jj-1]=*(result_mie
296         +2);
297         for_product[3][jj-1]=*(result_mie+3); for_product[4][jj
298           -1]=*(result_mie+4); for_product[5][jj-1]=*(result_mie
299             +5);}
300       if(mm===-1) {for_product[6][jj-1]=*(result_mie); for_product
301         [7][jj-1]=*(result_mie+1); for_product[8][jj-1]=*(
302           result_mie+2);
303           for_product[9][jj-1]=*(result_mie+3); for_product[10][jj

```

```

        -1]=*(result_mie+4); for_product[11][jj-1]=*(  

        result_mie+5);}  

296    } }  

297  

298 // Field calculation.  

299 int number_m1; complex<double> PRODUCTEr = 0, PRODUCTEt = 0,  

        PRODUCTEp = 0, PRODUCTPr = 0, PRODUCTPt = 0, PRODUCTPp =  

        0, PRODUCTEr_in = 0, PRODUCTEt_in = 0, PRODUCTEp_in = 0,  

        PRODUCTPr_in = 0, PRODUCTPt_in = 0, PRODUCTPp_in = 0,  

        PRODUCTEr_inc = 0, PRODUCTEt_inc = 0, PRODUCTEp_inc = 0,  

        MULTI1=0, MULTI2=0, MULTI3=0, MULTI4=0, MULTI5=0;  

300  

301 for(int jj1 = 1; jj1<=number_j; jj1++) {  

302     CC=0.5*pow(img,jj1)*sqrt(4.*PI*(2*jj1+1));  

303     complex<double> varR=0, varT=0, varP=0;  

304  

305     for(int mm1 = -1; mm1<=1; mm1+=2) { if(mm1==1) {number_m1=0;}  

            else{number_m1=6;}  

306     // E_inc  

307     PRODUCTEr_inc+=CC*alpha2*(img/sp_r)*sqrt(jj1*(jj1+1))*b_inc(  

            jj1,mm1)*j(jj1,x)*Y(jj1,mm1,theta,phi);  

308     PRODUCTEt_inc+=CC*(alpha2*(img/sp_r)*b_inc(jj1,mm1)*RBj_prime  

            (jj1,x)*Yt1(jj1,mm1,theta,phi)+a_inc(jj1,mm1)*j(jj1,x)*Yt0  

            (jj1,mm1,theta,phi));  

309     PRODUCTEp_inc+=CC*(alpha2*(img/sp_r)*b_inc(jj1,mm1)*RBj_prime  

            (jj1,x)*Yp1(jj1,mm1,theta,phi)+a_inc(jj1,mm1)*j(jj1,x)*Yp0  

            (jj1,mm1,theta,phi));  

310     // E_in  

311     PRODUCTEr_in+=CC*(alpha1*(img/sp_r)*sqrt(jj1*(jj1+1))*  

            for_product[number_m1+3][jj1-1]*j(jj1,m*x))*Y(jj1,mm1,

```

```

    theta,phi);

312 PRODUCTet_in+=CC*(alpha1*(img/sp_r)*for_product[number_m1+3][
    jj1-1]*RBj_prime(jj1,m*x)*Yt1(jj1,mm1,theta,phi)+a_in(jj1,
    mm1)*j(jj1,m*x)*Yt0(jj1,mm1,theta,phi));

313 PRODUCTEp_in+=CC*(alpha1*(img/sp_r)*for_product[number_m1+3][
    jj1-1]*RBj_prime(jj1,m*x)*Yp1(jj1,mm1,theta,phi)+a_in(jj1,
    mm1)*j(jj1,m*x)*Yp0(jj1,mm1,theta,phi));

314 // P_in

315 PRODUCTPr_in+=CC*(alpha1*(img/sp_r)*sqrt(jj1*(jj1+1))*[
    for_product[number_m1+5][jj1-1]*j(jj1,m*x))*Y(jj1,mm1,
    theta,phi);

316 PRODUCTPt_in+=CC*(alpha1*(img/sp_r)*for_product[number_m1+5][
    jj1-1]*RBj_prime(jj1,m*x)*Yt1(jj1,mm1,theta,phi)+[
    for_product[number_m1+4][jj1-1]*j(jj1,m*x)*Yt0(jj1,mm1,
    theta,phi));

317 PRODUCTPp_in+=CC*(alpha1*(img/sp_r)*for_product[number_m1+5][
    jj1-1]*RBj_prime(jj1,m*x)*Yp1(jj1,mm1,theta,phi)+[
    for_product[number_m1+4][jj1-1]*j(jj1,m*x)*Yp0(jj1,mm1,
    theta,phi));

318 // E_out

319 varR+=CC*(alpha2*(img/sp_r)*sqrt(jj1*(jj1+1))*(b_inc(jj1,mm1)
    *j(jj1,x)+for_product[number_m1][jj1-1]*h1(jj1,x)))*Y(jj1,
    mm1,theta,phi);

320 varT+=CC*(alpha2*(img/sp_r)*(b_inc(jj1,mm1)*RBj_prime(jj1,x)+[
    for_product[number_m1][jj1-1]*RBh_prime(jj1,x))*Yt1(jj1,
    mm1,theta,phi)+(a_inc(jj1,mm1)*j(jj1,x) +a_sc(
    jj1,mm1)*h1(jj1,x))*Yt0(jj1,mm1,theta,phi));

321 varP+=CC*(alpha2*(img/sp_r)*(b_inc(jj1,mm1)*RBj_prime(jj1,x)+[
    for_product[number_m1][jj1-1]*RBh_prime(jj1,x))*Yp1(jj1,
    mm1,theta,phi) +(a_inc(jj1,mm1)*j(jj1,x)+a_sc(jj1,mm1)*h1(

```

```

        jj1,x))*Yp0(jj1,mml,theta,phi));
322 // P_out
323 PRODUCTPr+=CC*alpha2*(img/sp_r)*sqrt(jj1*(jj1+1))*(

    for_product[number_m1+2][jj1-1]*h1(jj1,x))*Y(jj1,mml,theta
    ,phi);
324 PRODUCTPt+=CC*(alpha2*(img/sp_r)*(for_product[number_m1+2][

        jj1-1]*RBh_prime(jj1,x))*Yt1(jj1,mml,theta,phi)+(
    for_product[number_m1+1][jj1-1]*h1(jj1,x))*Yt0(jj1,mml,
    theta,phi));
325 PRODUCTPp+=CC*(alpha2*(img/sp_r)*(for_product[number_m1+2][

        jj1-1]*RBh_prime(jj1,x))*Yp1(jj1,mml,theta,phi) +(
    for_product[number_m1+1][jj1-1]*h1(jj1,x))*Yp0(jj1,mml,
    theta,phi));
326 }
327 PRODUCTEr+=varR;
328 PRODUCTEt+=varT;
329 PRODUCTEp+=varP;
330 if(jj1==1){MULTI1=varR*conj(varR)+varT*conj(varT)+varP*conj(
    varP);}
331 if(jj1==2){MULTI2=varR*conj(varR)+varT*conj(varT)+varP*conj(
    varP);}
332 if(jj1==3){MULTI3=varR*conj(varR)+varT*conj(varT)+varP*conj(
    varP);}
333 if(jj1==4){MULTI4=varR*conj(varR)+varT*conj(varT)+varP*conj(
    varP);}
334 if(jj1==5){MULTI5=varR*conj(varR)+varT*conj(varT)+varP*conj(
    varP);}
335 } // END: Field calculation.
336
337 PRODUCT_EP = PRODUCTEr*conj(PRODUCTPr)+PRODUCTEt*conj(

```

```

        PRODUCTPt)+PRODUCTEp*conj(PRODUCTPp);

338 PRODUCT_EE = PRODUCTEr*conj(PRODUCTEr)+PRODUCTEt*conj(
        PRODUCTEt)+PRODUCTEp*conj(PRODUCTEp);

339

340 PRODUCT_EP_in = PRODUCTEr_in*conj(PRODUCTPr_in)+PRODUCTEt_in*
        conj(PRODUCTPt_in)+PRODUCTEp_in*conj(PRODUCTPp_in);

341 PRODUCT_EE_in = PRODUCTEr_in*conj(PRODUCTEr_in)+PRODUCTEt_in*
        conj(PRODUCTEt_in)+PRODUCTEp_in*conj(PRODUCTEp_in);

342

343 eps1 = eps_inf + conj(PRODUCT_EP_in)/PRODUCT_EE_in;
344 eps2 = eps2_0*eps_0 + 2.*conj(PRODUCT_EP)/PRODUCT_EE;
345
346 polarizability = (eps1-eps2)/(eps1+2.*eps2);
347
348 N = RK4( N, 1./T1, -Nf/T1-img*(PRODUCT_EP-conj(PRODUCT_EP))
        *2.*PI/(n_density*h*ome_pl) );
349
350 double c1_p = 774.1493093877559; // |External electric field
        |^2 when G=0.
351 double c2_p = c1_p*eps_0;
352 double c3_p = c2_p*eps_0;
353
354 if(it==it_max){file7<<ome_eV<<" "<<real(polarizability)<<" "
        <<imag(polarizability)<<"\n";}

355 cout<<"Final N: "<<N<<endl;
356 cout<<"Final E: "<<real(PRODUCT_EE)/c1_p<<endl;
357 cout<<"MULTI: "<<real(MULTI1)<<" "<<real(MULTI2)<<" "<<real(
        MULTI3)<<" "<<real(MULTI4)<<" "<<real(MULTI5)<<endl;
358 cout<<"EPS A C: "<<eps1_exact<<" "<<eps1<<" "<<eps2_exact<<" "

```

```

    "<<eps2<<endl;

360
361     file6<<it*time_step<<" " << scientific<<setprecision(10)<<
        real( PRODUCTPr*conj(PRODUCTPr)+PRODUCTPt*conj(PRODUCTPt)+
        PRODUCTPp*conj(PRODUCTPp) )/c3_p   <<" " << imag(PRODUCT_EP)
        /c2_p <<" " <<real(PRODUCT_EE)/c1_p<<" " <<real(MULTI1)/c1_p
        <<" " <<real(MULTI2)/c1_p<<" " <<real(MULTI3)/c1_p<<" " <<
        real(MULTI4)/c1_p<<" " <<real(MULTI5)/c1_p<<" " <<real(eps1)
        /eps_0<<" " <<imag(eps1)/eps_0<<" " <<real(eps2)/eps_0<<" "
        <<imag(eps2)/eps_0<<"\n";
362
363 } // END: Analysis.
364
365     file3.close(); file4.close(); file5.close(); file6.close();
            file7.close(); // The files are closed.
366     clock_t end=clock(); // Time measurement ends.
367     double elapsed_secs=double(end-begin)/CLOCKS_PER_SEC; cout<<""
            \nExecution time (min): "<<elapsed_secs/60<<endl; //
            Execution time.
368     cout<<"\nAnalysis for G = "<<G<<" theta = "<<theta*180./PI<<""
            phi = "<<phi*180./PI<<" ome = "<<ome_eV<<"\n"<<endl;
369
370     cout<<"plot \' "<<name_file3_ome<<"\' w 1 lw 2 title \'N\'"<<endl;
371     cout<<"plot \' "<<name_file6_ome<<"\' u 1:4 w 1 lw 2 title \'|E
            |^2\'"<<endl;
372     cout<<"plot \' "<<name_file6_ome<<"\' u 1:10 w 1 lw 2 title \'Re(
            eps1)/Re(eps1_{SS})\', \'\' u 1:11 w 1 lw 2 title \'Im(eps1)/
            Im(eps1_{SS})\'"<<endl;
373     cout<<"plot \' "<<name_file6_ome<<"\' u 1:12 w 1 lw 2 title \'Re(
            eps2)/Re(eps2_{SS})\', \'\' u 1:13 w 1 lw 2 title \'Im(eps2)/
            Im(eps2_{SS})\'"<<endl;

```

```

    Im(eps2_{SS}))\' " << endl;
374 cout << "plot \' " << name_file7_ome << "\' u 1:2 w p pt 7 ps 2 title \
    Re(alpha)\', \' \' u 1:3 w p pt 7 ps 2 title \' Im(alpha)\' " <<
    endl;
375
376 } // END: main

```

12.2 Example of input file

This would be the content of file `in/nanosphere-eV.dat`, where the radius of the nanosphere a (in nm), $\hbar\Delta$ (in eV), the resonance frequency $\hbar\omega_{21}$ (in eV), the gain G , and the minimum and maximum value of the incident field frequency $\hbar\omega$ (in eV) are specified.

| | | | | | | |
|---|-----|------|------------|--------|-------|-------|
| 1 | 10 | 0.2 | 3.19981733 | -0.065 | 3.1 | 3.3 |
| 2 | #r1 | Dome | ome_0 | G | omemi | omema |
